NASA/TM– 20240002776

Structural Analysis and Testing of Multi-nut Joint for TriTruss Structure

Kyongchan Song, Clarence E. Stanfield, Judith J. Watson, and Olive R. Stohlman
Langley Research Center, Hampton, Virginia

May 2024

NASA STI Program Report Series

Since its founding, NASA has been dedicated to the advancement of aeronautics and space science. The NASA scientific and technical information (STI) program plays a key part in helping NASA maintain this important role.

The NASA STI program operates under the auspices of the Agency Chief Information Officer. It collects, organizes, provides for archiving, and disseminates NASA's STI. The NASA STI program provides access to the NTRS Registered and its public interface, the NASA Technical Reports Server, thus providing one of the largest collections of aeronautical and space science STI in the world. Results are published in both non-NASA channels and by NASA in the NASA STI Report Series, which includes the following report types:

- TECHNICAL PUBLICATION. Reports of completed research or a major significant phase of research that present the results of NASA Programs and include extensive data or theoretical analysis. Includes compilations of significant scientific and technical data and information deemed to be of continuing reference value. NASA counterpart of peer-reviewed formal professional papers but has less stringent limitations on manuscript length and extent of graphic presentations.

- TECHNICAL MEMORANDUM. Scientific and technical findings that are preliminary or of specialized interest, e.g., quick release reports, working papers, and bibliographies that contain minimal annotation. Does not contain extensive analysis.

- CONTRACTOR REPORT. Scientific and technical findings by NASA-sponsored contractors and grantees.

- CONFERENCE PUBLICATION. Collected papers from scientific and technical conferences, symposia, seminars, or other meetings sponsored or co-sponsored by NASA.

- SPECIAL PUBLICATION. Scientific, technical, or historical information from NASA programs, projects, and missions, often concerned with subjects having substantial public interest.

- TECHNICAL TRANSLATION. English-language translations of foreign scientific and technical material pertinent to NASA's mission.

Specialized services also include organizing and publishing research results, distributing specialized research announcements and feeds, providing information desk and personal search support, and enabling data exchange services.

For more information about the NASA STI program, see the following:

- Access the NASA STI program home page at http://www.sti.nasa.gov

- Help desk contact information:

https://www.sti.nasa.gov/sti-contact-form/
and select the "General" help request type.

NASA/TM– 20240002776

Structural Analysis and Testing of Multi-nut Joint for TriTruss Structure

Kyongchan Song, Clarence E. Stanfield, Judith J. Watson, and Olive R. Stohlman
Langley Research Center, Hampton, Virginia

National Aeronautics and
Space Administration

Langley Research Center
Hampton, Virginia 23681-2199

May 2024

Available from:

NASA STI Program / Mail Stop 050
NASA Langley Research Center
Hampton, VA 23681-2199

Table of Contents

List of Figures

List of Tables

Nomenclature

EA	Joint equivalent axial stiffness
EI	Joint equivalent bending stiffness
FEM	Finite element model
iSAT	in-Space Assembled Telescope
kips	kilo pound per square inch
LaRC	NASA Langley Research Center
MTT	Material Testing Technology
PASS	Precision Assembled Space Structure
LVDT	Linear Variable Differential Transformer

Abstract

Axial and bending tests for a multi-nut joint in the TriTruss structure were conducted at NASA Langley Research Center (LaRC). This report describes the test procedures used for the axial and bending tests of the multi-nut joint, along with the test results. The joint's equivalent axial stiffness (EA) and equivalent bending stiffness (EI) were characterized based on these test results and are presented in this report. Additionally, finite element models (FEMs) of the axial and bending test specimens were developed, and the predicted axial and bending responses of the multi-nut joint were compared and validated with the test results.

1.0 Introduction

The Precision Assembled Space Structure (PASS) project has the goal to develop a structural design and to demonstrate an autonomous assembly method for a 20-meter telescope support structure. The structural shape is based on the in-space assembled telescopes (iSAT) study [1], which details a 20-meter diameter telescope parabolic mirror built up from individual truss units called TriTrusses (Figure 1).

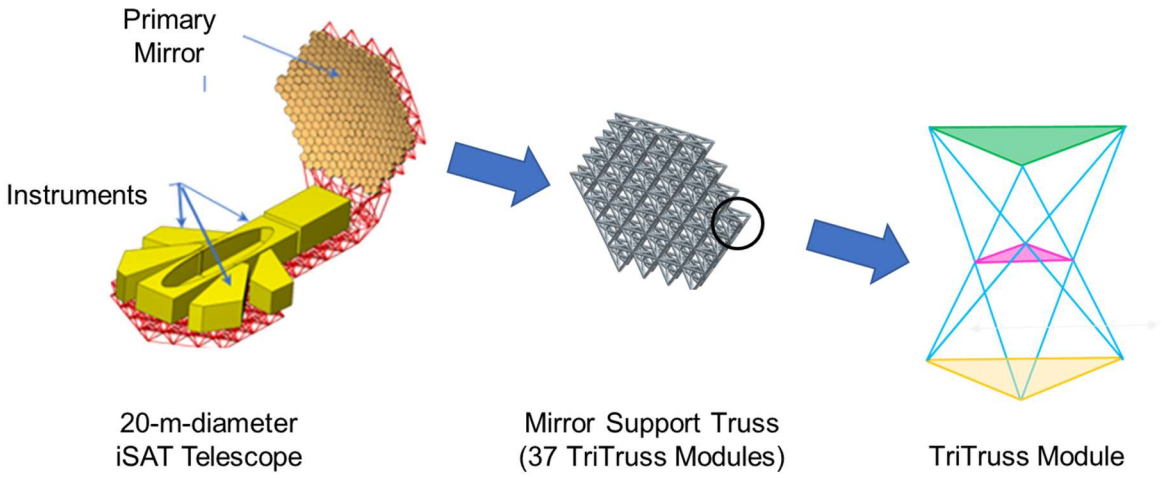

Figure 1. iSAT support structure and TriTruss Module.

The TriTruss [2,3,4] is an innovative structural module that has been developed by researchers at NASA Langley Research Center (LaRC) for near-zero-g, i.e., the gravitational force experienced in near Earth orbit, in-space-assembled telescopes and platforms for science and communications. Some of the innovative features of the TriTruss include very compact packaging for launch, the possibility of staged packaging, simple robotic deployment, ease of embedding payload components, an innovative structural connector that has linear structural performance, ease of module-to-module robotic assembly, design versatility, and ease of customizing its design for specific applications [2]. For the PASS project, a doubly curved 20-meter telescope support structure will be constructed by 37 identical wedge-shaped TriTruss modules. In order to achieve a doubly curved structure comprised of uniform TriTruss modules, gaps are intentionally left at

the nodes between connecting modules. These gaps are filled using uniquely shaped nodal connectors called **multi-nuts**, which connect adjacent modules using fasteners [5]. A wedge-shaped TriTruss module and the multi-nut joint which connects corner nodes of three TriTruss modules are shown in Figure 2.

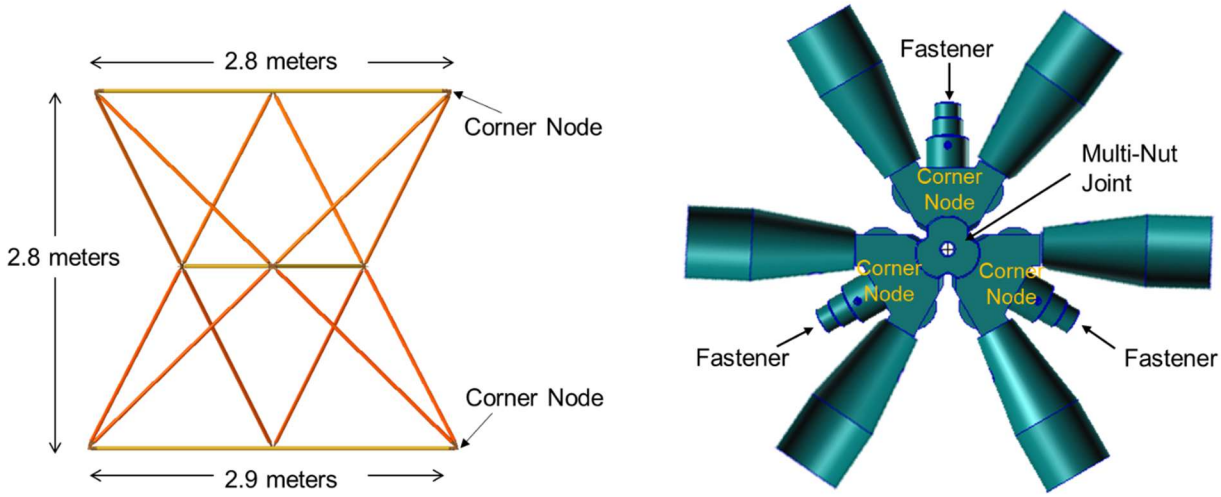

Figure 2. The wedge-shaped TriTruss module and multi-nut joint.

In the initial trade study [4], the governing equations for mass, dimensions, and frequency of a multi-ring telescope support structure were developed. The governing equations for the multi-ring telescope support structure were used to perform rapid and realistic parametric trade studies, allowing major drivers in precision reflector designs to be determined. Finite element models (FEMs) of TriTruss modules were developed with general Timoshenko (shear flexible) beam elements. Individual module FEM was connected by rigid points at the multi-nut locations to construct a multi-ring telescope support structure. Frequency and static analyses were performed on these FEMs to investigate the overall structural response of TriTruss modules throughout the assembly process and to support various tests involving robotic operations. Although the existing governing equations and FEMs utilizing beam elements worked well in facilitating trade studies and providing preliminary structural response for the multi-ring telescope support structure, an improved analytical approach for the multi-nut joint model is essential for a comprehensive analysis of the multi-ring telescope support structure.

In order to characterize the multi-nut joint with connected nodes of adjacent TriTruss modules, tests were developed to characterize the joint's equivalent axial stiffness (EA) and equivalent bending stiffness (EI). FEMs of axial and bending test specimens were developed for prediction and test correlation. The axial test was developed to determine equivalent EA based on the axial test program summarized in Ref [6]. The bending test plan was developed to determine equivalent EI based on Ref [6,7]. Axial and bending tests were performed at LaRC and measured structural response of the axial and bending test specimens, including forces and displacements, were compared with the predictions obtained from FEM.

In this report, descriptions of the axial and bending test as well as comparison of selected test results with predicted results are given in Section 2 and 3, respectively. Concluding remarks are presented in Section 4.

2.0 Multi-Nut Joint Axial Test

The axial test series for the multi-nut joint consisted of a calibration test and the multi-nut joint specimen test. First, a calibration test was performed using the calibration test specimen with a known stiffness value in place of the multi-nut. The objectives of a calibration test were to verify the axial test setup, test procedures, provide reference data, and to demonstrate the reliability of the axial test equipment. After the calibration test, five axial test specimens fabricated with the multi-nut joints were tested at room temperature. The objectives of the axial test of the multi-nut joint were:

1. Evaluate the multi-nut joint for axial performance and provide reference data.
2. Determine the installation torque value of the attachment fastener to achieve linear load-displacement response in the operation load range.
3. Determine an equivalent EA over the two corner nodes and multi-nut joint based on the axial test results.
4. Provide multi-nut joint performance results to validate the finite element model of a multi-nut joint.

In this section, the axial test setup, the results of calibration and multi-nut joint axial test, modeling of a multi-nut axial test specimen, the calculated axial stiffness of the multi-nut joint, and the summary of the axial test are provided in this section.

2.1 Axial Calibration Test and Analysis

The axial tests were conducted using the MTS Insight 30 EL axial tension-compression load frame, equipped with the 1 kips in-line load cell. In both the axial calibration and the multi-nut joint test specimens, applied maximum tension and compression loads were ± 500 lbs. The maximum tension and compression test loads were obtained from the 110-inch (2.8-meter) composite strut test which was performed to test the bonding strength between composite tube and end fittings and to obtain the strut buckling load. The first calibration test revealed a flaw in the test setup. This first measurement, the resulting correction to the test setup, and the updated test measurement are presented in this section.

The calibration test specimen was fabricated utilizing a 6061 aluminum tube having a total length of 14.0 inch, an outer diameter of 2.0 inch, and a wall thickness of 0.5 inch. The calibration test specimen had a 9.5-inch test section, a 2.0-inch threaded sections, and a 0.25-inch tab between the test section and thread section at both ends. The design of the calibration test specimen is shown using the fabrication drawing, Figure A-1 of Appendix A. As shown in Figure 3, the measurement plates were placed above and below the test section. Three LVDTs (Linear Variable Differential Transformers) were positioned between the plates as the specimen was loaded. The three LVDTs were evenly spaces at 120 degrees and 1 inch in from the outer edge of the measurement plate, as shown in Figure 3.

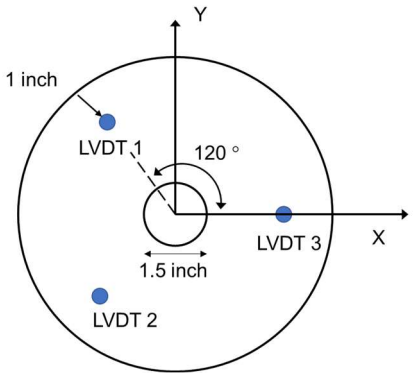

Figure 3. The measurement plate with three LVDT locations.

As shown in Figure 4, a custom jam nut, made using a medium-strength steel hex nut, locks the measurement plates in place between the test section and the load machine couplings. The initial test setup with the calibration test specimen is shown in Figure 4.

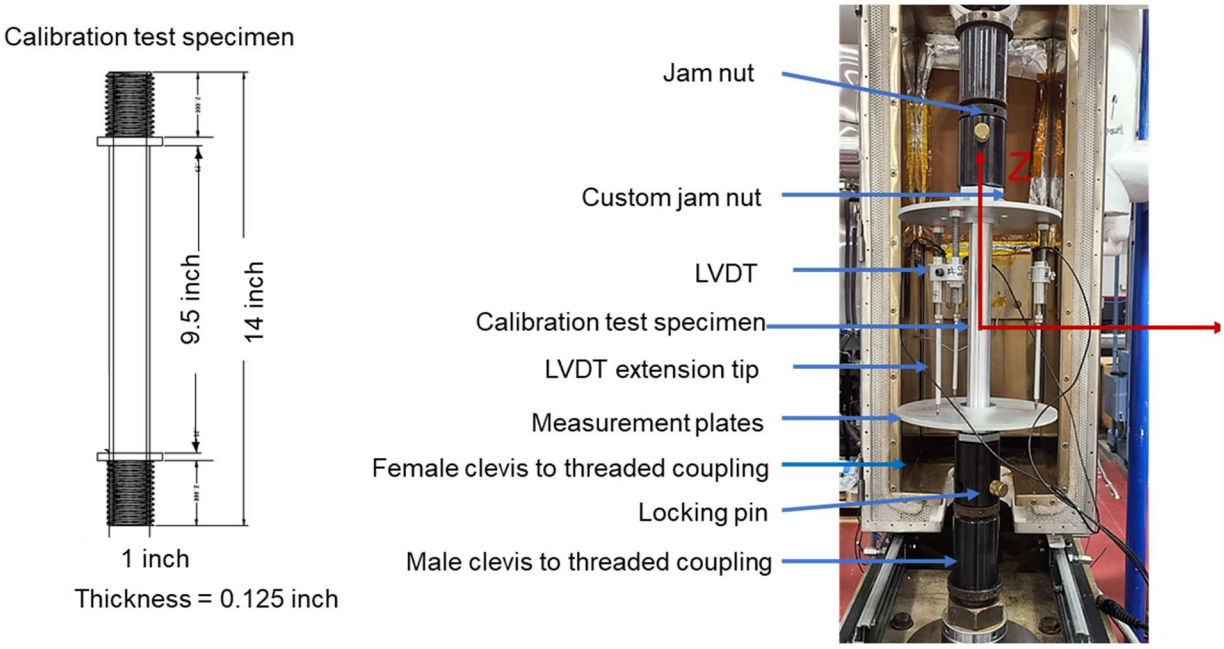

a) Calibration test specimen

b) The initial test setup including the calibration test specimen

Figure 4. The calibration test specimen and the initial test setup.

The FEMs of the test specimen and the test fixture are shown in Figure 5. For test-analysis comparisons, the FEMs of the calibration test specimen and test fixture were developed using Abaqus C3D8 solid elements [8]. Threaded sections of the test specimens and the load machine female clevis were connected by the tie constraint. Contact boundary conditions were applied to contact surfaces between test specimen tabs and measurement plates. The top and bottom nodes

of both female clevises were attached by kinematic constraints to reference nodes. The bottom reference node was fixed, effectively simulating the clamped boundary condition of the bottom male clevis. For calibration test, axial displacement was applied at the top reference node, simulating the top male clevis in either tension or compression.

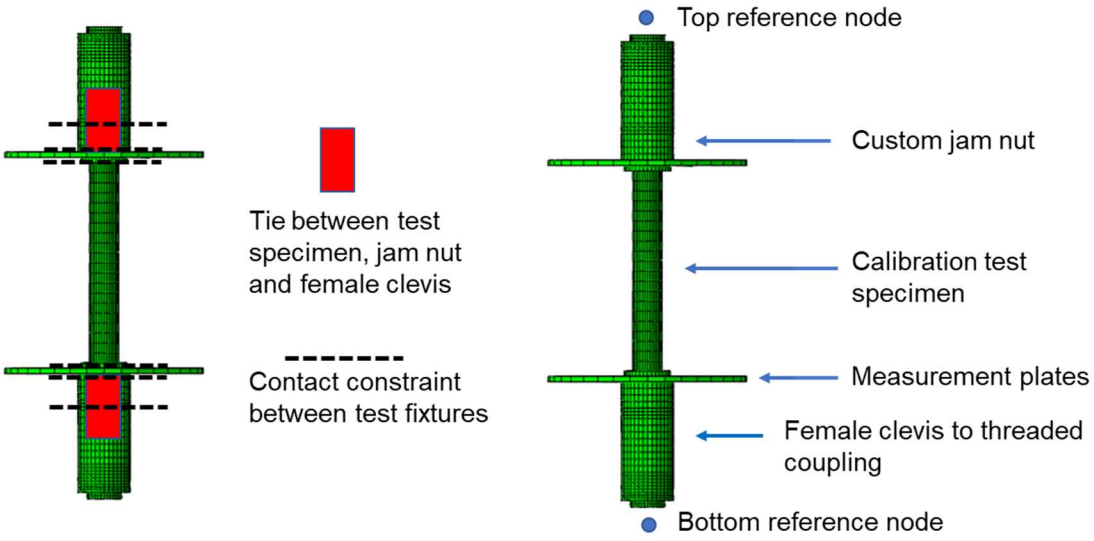

Figure 5. Finite element model of the test specimen and the test fixture.

Static analyses were performed on the FEM subjected to the maximum axial tension and compression loads. The load versus average measured displacement of three LVDTs, henceforth referred to as the load-displacement response, were compared with the predicted pretest results of the FEM and closed-form solution. The test results, predicted pretest results of FEM, and closed-form solution are shown in Figure 6.

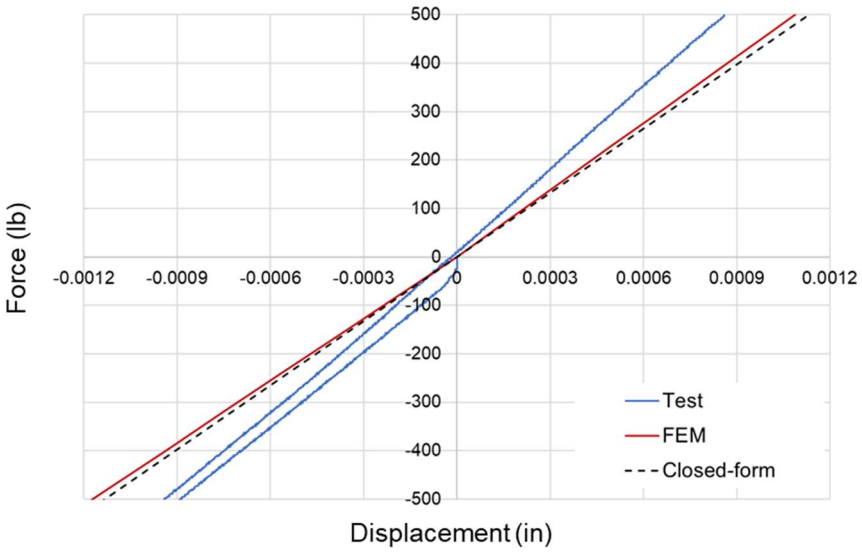

Figure 6. Test and analytical results of load versus measured displacement between two measurement plates.

As shown in Figure 6, the predicted pretest results and closed form solutions were consistent with each other, while the test results show a stiffer load-displacement response. Examining three individual LVDT results, shown in Figure 7, one of the LVDT results had an opposite sign relative to the other two LVDT results. Based on the individual LVDT results, it was noticed that the measurements plates were not secured to the calibration test specimen and tilted during the axial test.

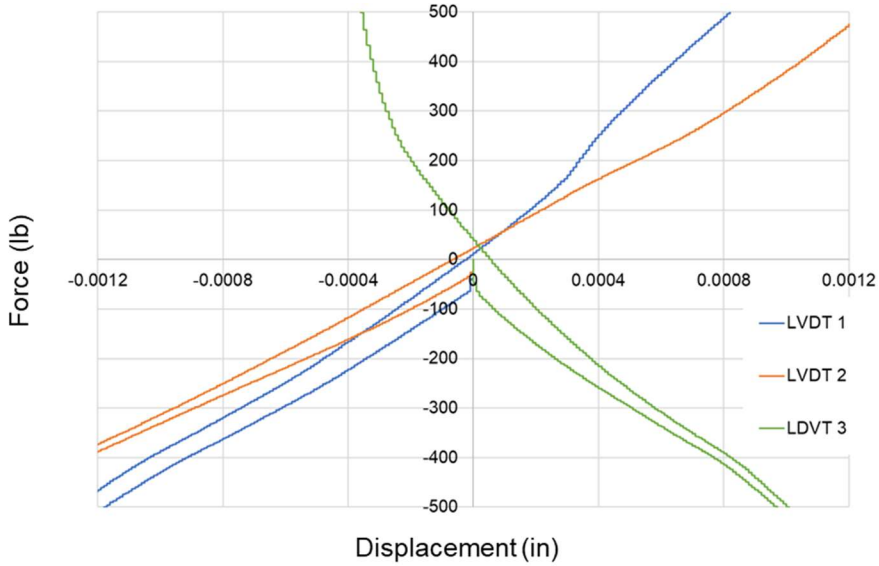

Figure 7. The load versus measured displacement of three LVDTs.

Based on the initial calibration test results, the following recommendations were made to prevent movement of measurement plates.

- Refabricate the measurement plate with smaller tolerance on the center 1.5 inch hole.
- Replace custom jam nuts with material testing technology (MTT) LN46 jam nut.
- Remove the flexible LVDT tip extender and add a stiff rod to the end of LVDT.

The modified axial test setup is shown in Figure 8 with the initial axial test setup.

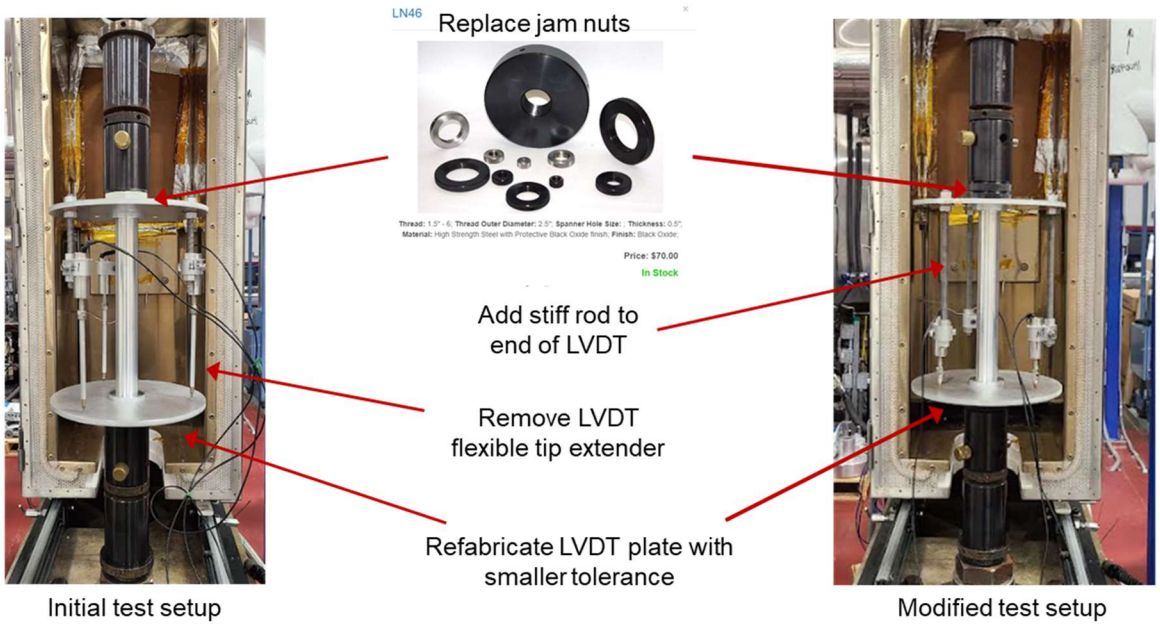

Figure 8. Modified axial test setup.

Individual LVDT results obtained from the modified axial test setup are shown in Figure 9 and indicated that all three LVDT results showed the same sign and similar linear trend of the load-displacement response. The load-displacement response obtained from the modified axial test setup was compared with the predicted pretest results and closed-form solution in Figure 10. The comparison results of test, predicted pretest results, and closed-form solution indicated that the modified test setup could accurately obtain measured displacements between two measurement plates and demonstrated the reliability of the axial test setup.

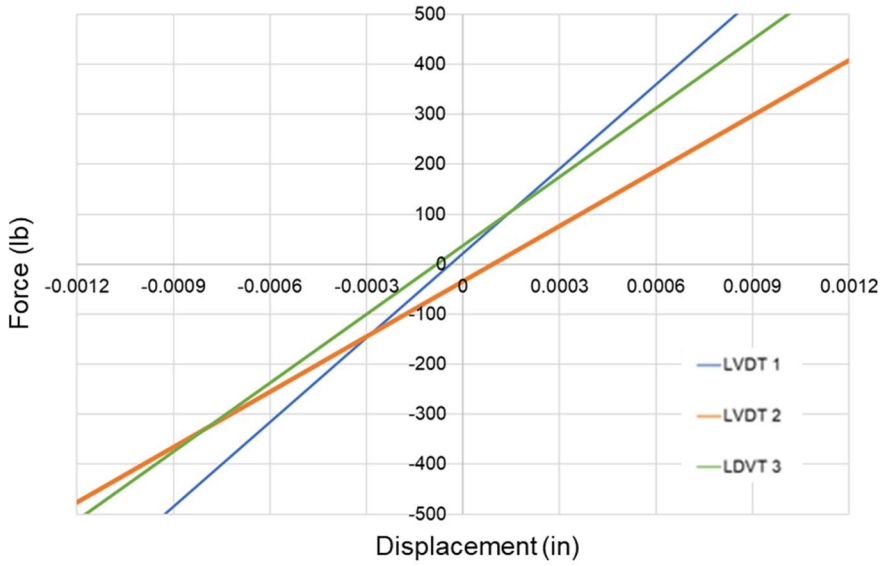

Figure 9. The load versus measured displacement of three LVDTs (modified test setup).

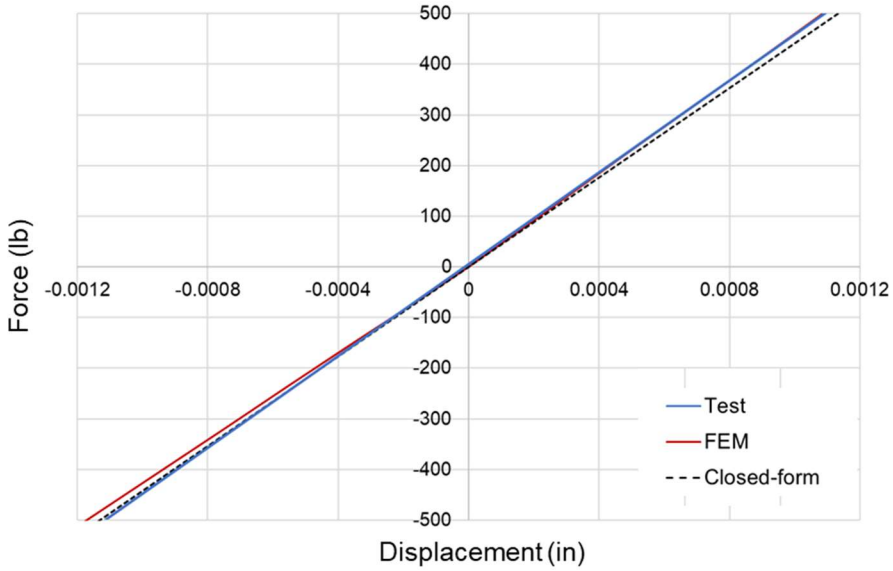

Figure 10. Test and analytical results of load versus measured displacement between two measurement plates (modified test setup).

2.2 Multi-Nut Axial Test and Analysis

A test specimen with a 7.94-inch-long joint section composed of three corner nodes and a multi-nut joint, was designed for the multi-nut axial test. In a TriTruss module, each corner node consists of two diagonal and two in-plane bonded sections, and each bonded section has a conical and cylinder bonded section. For the axial test specimen, corner nodes were modified to fit in the test fixture by eliminating two diagonal bonding sections. Specially designed thread adapters were bonded to both end cylinder bonding sections of the test specimen. The design of the thread adapter

is shown in the fabrication drawing, Figure A-2 of Appendix A. The modified corner node with the threaded adapter is shown in Figure 11.

The diameter of the multi-nut joint is 1.15 inch, and the height is 0.71 inch with 10-degree taper angle. Three fastener holes in the multi-nut joint are placed 120 degrees apart and aligned with a fastener hole in each corner node. The geometry detail of the multi-nut joint is shown in Figure 12.

Three modified corner nodes were connected to a multi-nut joint by M6 fasteners (45 mm/1.77-inch-long steel socket head screws). Then, the test specimen was inserted into female clevis. The final test specimen and the axial test setup are shown in Figure 13.

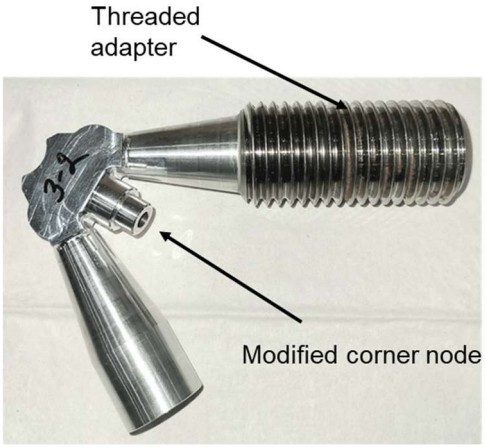

Figure 11. Modified corner node and threaded adapter.

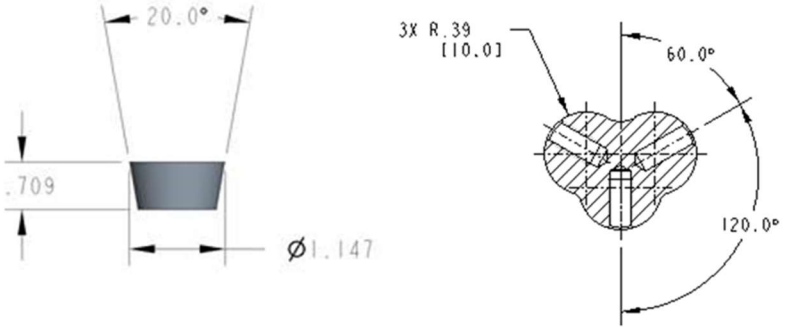

Figure 12. The multi-nut joint design (units are in inches and degrees).

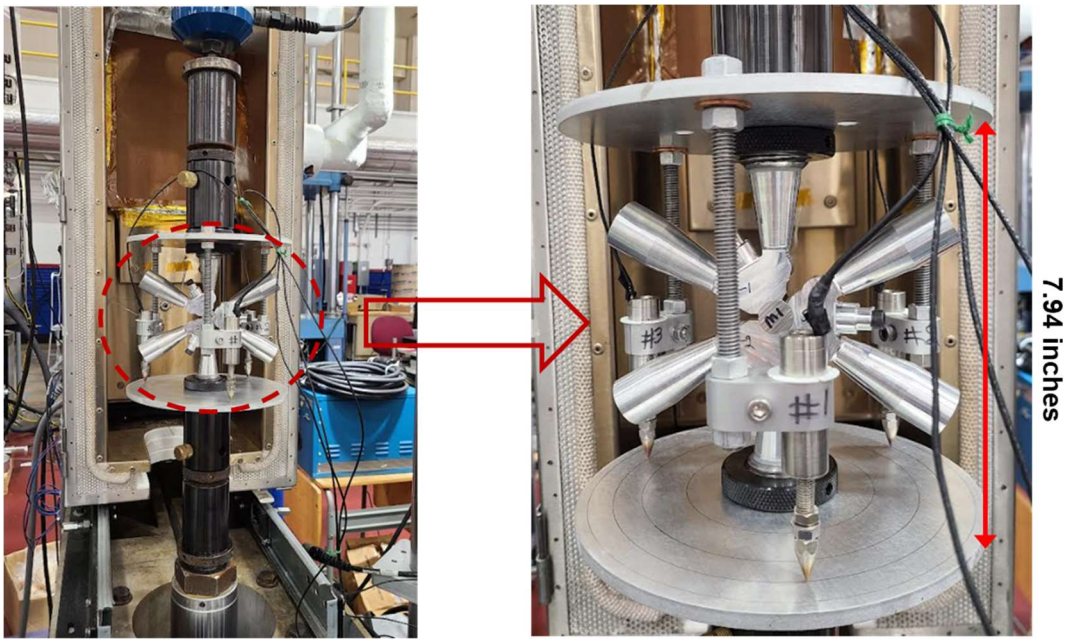

Figure 13. Multi-nut test specimen and test setup.

Five axial test specimens were fabricated utilizing a multi-nut and modified corner nodes. The fasteners were tightened with four different preload torque values (15 in-lb, 30 in-lb, 60 in-lb, 120 in-lb). Axial tests, using the modified test set-up developed in the axial calibration test, were performed on test specimens subjected to maximum tension and compression axial loads of 500 lb with a loading rate of 10 lb/sec. Each axial test consisted of three compression and tension loading cycles. The multi-nut test procedure was:

1. Zero to compression load (50 seconds)
2. Hold 10 seconds
3. Compression to zero (50 seconds)
4. Hold 10 seconds
5. Zero to tension (50 seconds)
6. Hold 10 seconds
7. Return to zero (50 seconds)
8. Repeat 2 more loading cycles

2.2.1 Multi-Nut Axial Test Results

In this section, the load-displacement responses of the multi-nut axial test specimens for different preload torque values are presented and discussed. Each test specimen result is denoted as Test_i_PT_j, where 'i' represents the test specimen number (i = 1 to 5) and 'j' represents the preload torque value (15 in-lb, 30 in-lb, 60 in-lb, 120 in-lb).

The load-displacement responses of two test specimens subjected to the preload torque of 15 in-lb are presented in Figure 14.

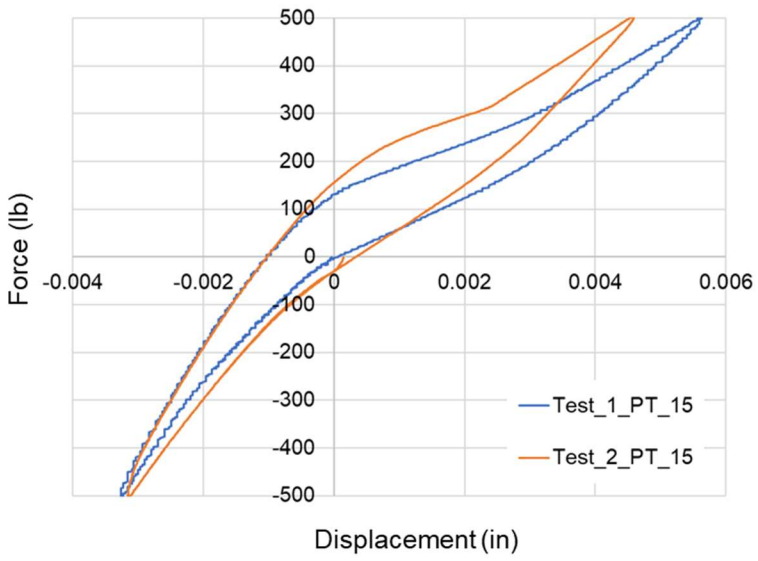

Figure 14. The load versus average measured displacement of multi-nut test specimens (Preload torque = 15 in-lb).

When preload torque of 15 in-lb was applied, the multi-nut test specimens exhibited a nonlinear load-displacement response for the axial testing condition. After the first compression cycle and as tension load was gradually applied to the test specimen, starting from the maximum compression load, the load-displacement response did not pass through the initial unloaded point. Instead, two changes in the slope were observed before reaching the maximum tension load condition. The test results indicated that a preload torque of 15 in-lb was insufficient to secure the fasteners, resulting in the multi-nut loosening from the corner nodes during axial loading. After the tests, post-test inspections of the test specimens clearly showed that the multi-nut had dislodged from the connected corner nodes.

The load-displacement responses of five test specimens subjected to the preload torque of 30 in-lb are presented in Figure 15.

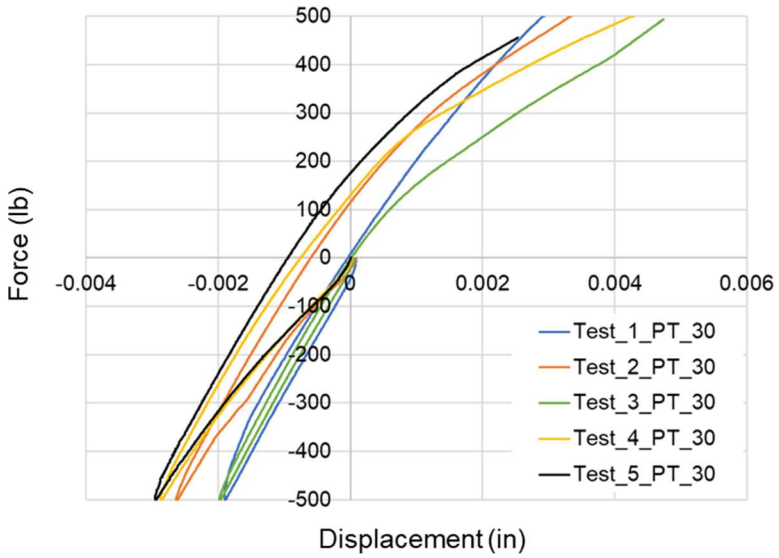

Figure 15. The load versus average measured displacement of multi-nut test specimens (Preload torque = 30 in-lb).

When a preload torque of 30 in-lb was applied, the multi-nut test specimens exhibited nonlinear load-displacement response for the axial testing conditions. Despite the improved load-displacement response under tension loading and no evidence of loosening of the multi-nut from corner nodes from the post-test inspection, the test results indicated that the preload torque of 30 in-lb was insufficient to secure the fasteners.

The load-displacement responses of five test specimens subjected to a preload torque of 60 in-lb are presented in Figure 16. When the preload torque of 60 in-lb was applied, the multi-nut test specimens exhibited linear load-displacement response curves for the axial load, except the test result of the specimen number 4, shown as the yellow curve in Figure 16. Post-test inspection indicated that the fastener hole in the multi-nut of test specimen number 4 did not have the design specified thread tolerance, and the fasteners were not fully engaged at the preload torque of 60 in-lb.

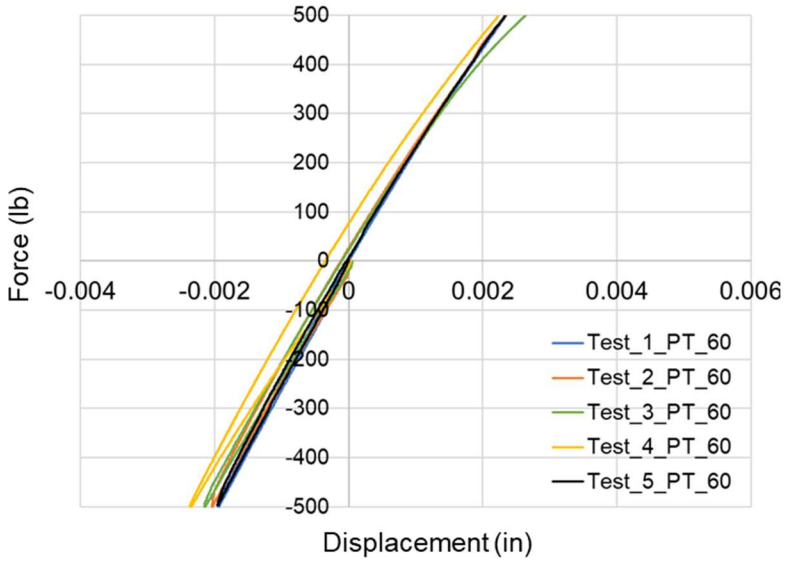

Figure 16. The load versus average measured displacement of multi-nut test specimens (Preload torque = 60 in-lb).

The CAD model of a multi-nut and corner node revealed that the 45 mm/1.77 inch long faster was engaged from a corner node into the multi-nut 0.173 inch deep, as shown in Figure 17.

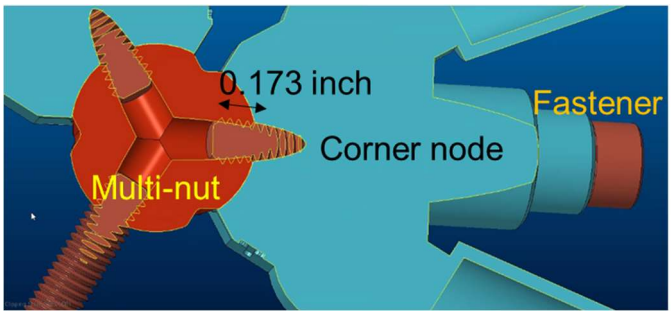

Figure 17. Fastener, corner node, and multi-nut engagement.

The test specimen number 4 was reassembled with 55 mm/2.17-inch-long fasteners and the preload torque 60 in-lb. The axial test was performed to study the effect of the fastener length on the load-displacement response of the multi-nut joint. The load-displacement responses of test specimen number 4 with different fasteners are presented in Figure 18. The load-displacement responses of the test specimen using longer fastener in Figure 18 showed that the nonlinear load-displacement response curve of the test specimen with 45 mm fasteners was improved to be more linear with 55 mm fasteners.

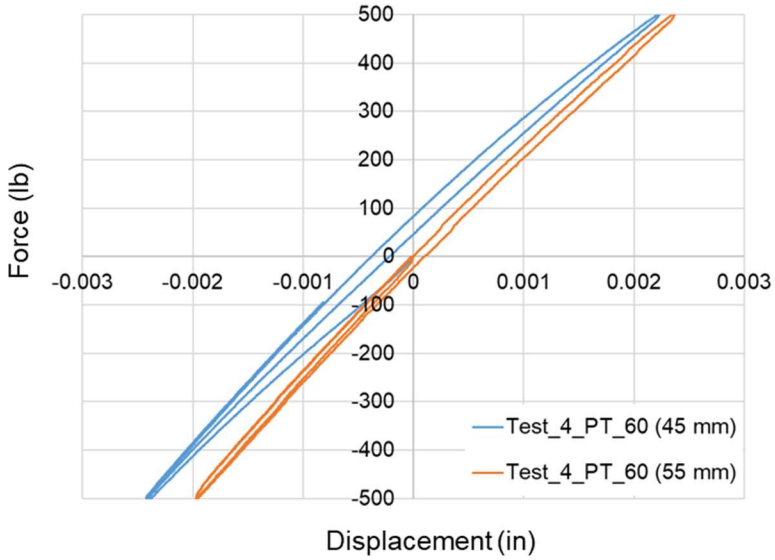

Figure 18. The load versus average measured displacement of multi-nut test specimens with different fasteners (Preload torque = 60 in-lb).

Test specimens number 4 and 5 were reassembled with 45 mm long fasteners and a preload torque of 120 in-lb. The axial test was repeated to study the effect of the higher preload on the load-displacement response of the multi-nut joint. The load-displacement response of two test specimens subjected to a preload torque of 120 in-lb are presented in Figure 19. When preload torque of 120 in-lb was applied, multi-nut test specimens exhibited linear load-displacement curves for the axial testing conditions.

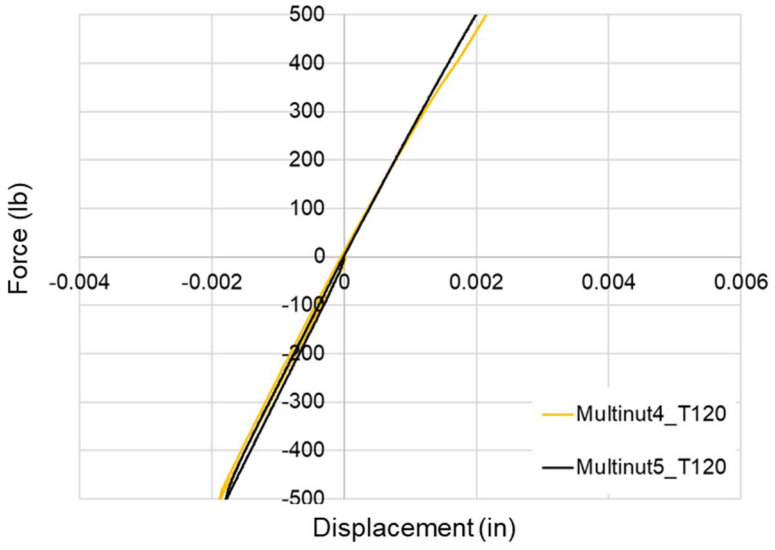

Figure 19. The load versus average measured displacement of multi-nut test specimens (Preload torque = 120 in-lb).

In this section, the test results were presented for the axial load-displacement response of the multi-nut joint for different preload torques and the lengths of the fastener. As shown in Figure 19, the 120 in-lb preload torque on the fastener achieved a nearly linear load-deflection performance over the majority of the applied axial load range with repeatability. As shown in Figure 17 and 18, while not as linear as the 120 in-lb fastener torque, the response for the 60 in-lb torque case was linear in the compressive loading and repeatable in both tension and compression loads. The change of fastener length, as demonstrated in Figure 18 with the fastener torque of 60 in-lbs, helped to improve the repeatability of test specimen number 4 and maintained the linear performance in compression, with the near linear performance in tension. Since one of the issues of the assembly of the TriTruss is the torque limit of the robot performing the assembly of the multi-nut joints, it is important to understand how the applied torque on the multi-nut fastener and the length of the fastener can determine the linear performance of the joint and thereby the structural performance of the assembled structure.

2.2.2 Finite Element Model of the Axial Test Speicmen

For test-analysis comparisons, FEM of the axial test specimen and test fixture were developed using Abaqus eight-node linear brick elements with reduced integration (C3D8R) and ten-node tetrahedral (C3D10) elements [8]. The total number of nodes is 67639 and total number of elements is 40980. The isotropic modulus of elasticity of 30 Msi and Poisson ratio of 0.3 were used for the FEM. Fasteners were modeled with two Abaqus general Timoshenko beam elements (B31). Both ends of fasteners were attached using kinematic constraints to multi-nut and corner nodes and the preload torque was applied to the middle node of the beam elements. The contact constraints were applied to the interfaces between the multi-nut and corner nodes. The FEMs of the multi-nut, corner nodes, and fasteners are shown in Figure 20.

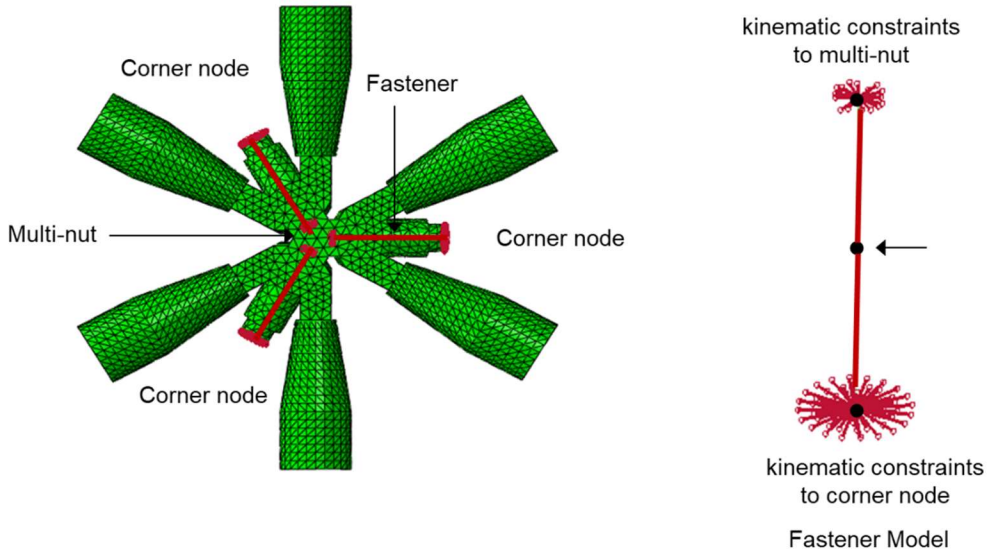

a) FEMs of the multi-nut and corner nodes b) FEM of fastener

Figure 20. Finite element model of multi-nut, corner nodes, and fasteners.

Threaded sections of the adapter and the female clevis were connected to each other by a tie constraint and contact boundary conditions were applied to contact surfaces between the test specimen tabs and measurement plates. The top and bottom nodes of both female clevises were attached using kinematic constraints to reference nodes. The bottom reference node was fixed, effectively simulating the clamped boundary condition of the test machine's bottom male clevis. For the axial test, an axial displacement was applied at the top reference node, simulating the test machine's top male clevis in either tension or compression loading. The FEM of the test specimen and the test fixture is shown in Figure 21.

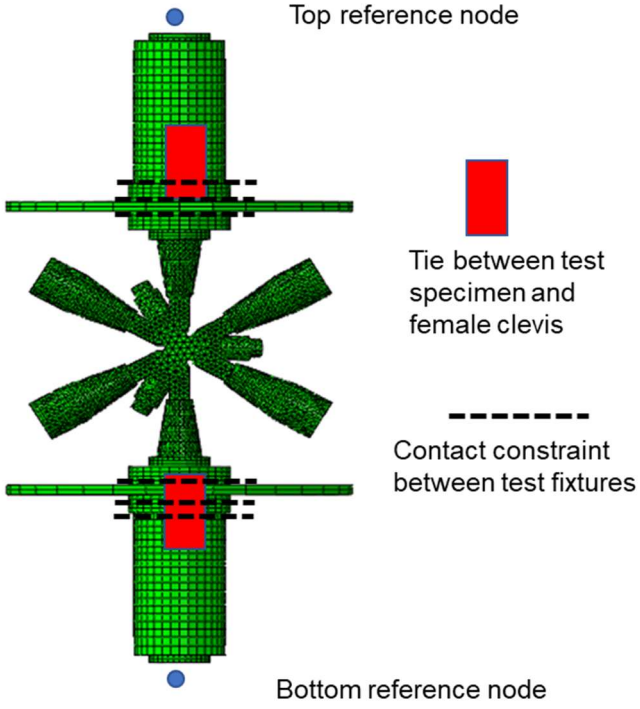

Figure 21. Finite element model of the axial test specimen and test fixture.

The load-displacement responses of FEMs with fastener preload torques of 30 in-lb and 60 in-lb are shown in Figure 22.

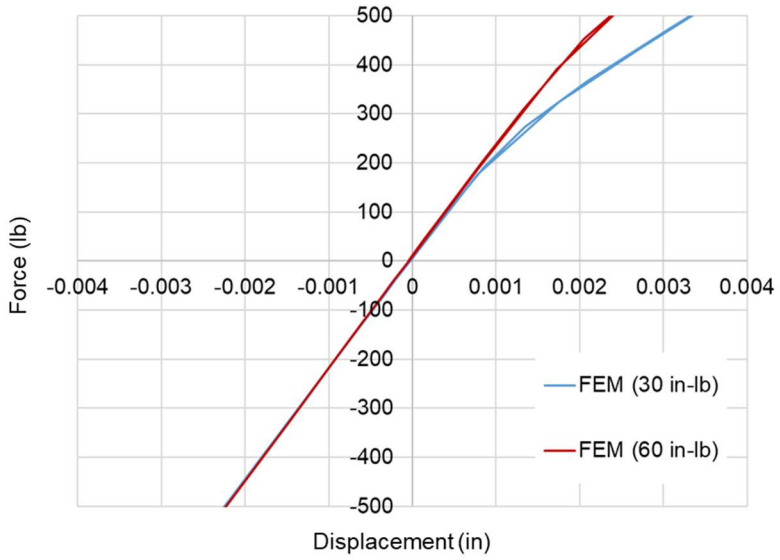

Figure 22. The predicted load versus average measured displacement of finite element model with preload torque = 30 in-lb and 60 in-lb.

As shown in Figure 22, the results of FEMs predicted similar linear load-displacement responses under compression loading, regardless of the preload torque values. In addition, as the applied load increased from the maximum compression load, the load-displacement response curve passed through the initial unloaded point. The effect of the preload torque on the load-displacement response curve of FEMs is shown for the tension loading conditions where both FEMs predicted a nonlinear response. Specifically, the FEM with a preload torque of 30 in-lb predicted a larger displacement (0.0033 in) compared to predicted displacement (0.0024 in) of the FEM with a preload torque of 60 in-lb at the maximum tension load.

In the static nonlinear analysis of the test specimen, fasteners were represented using beam elements. Then, the FEM of the multi-nut was assembled with FEMs of corner nodes using beam elements without leaving any gaps or clearances in the test specimen parts. In addition, the contact force between the fastener and fastener holes in multi-nut and corner nodes was not simulated. However, during the loading conditions, the actual test specimen underwent a settling phase that could result in the closure or opening of clearances in the fastener threads. If the preload torque applied to the fasteners was insufficient, this settling process could significantly affect the nonlinear load-displacement response of the test specimens. The effects of fastener settling became evident in the test results when the preload torque was below 60 in-lb.

The predicted load-displacement responses of FEM with a preload torque of 30 in-lb are shown with test results in Figure 23. The predicted load-displacement responses of FEM with preload torque of 60 in-lb are shown with test results in Figure 24. In Figure 23 and 24, solid color lines represent test results from different test specimens and the black dashed line represents the predicted results of FEM. A comparison between the predicted load-displacement response from the FEM and the test results revealed that when the preload torque was less than 60 in-lb, the predicted response of the FEM did not correlate well with the experimental results. However, when

the preload torque met or exceeded 60 in-lb, the predicted response of the FEM consistently matched the test results.

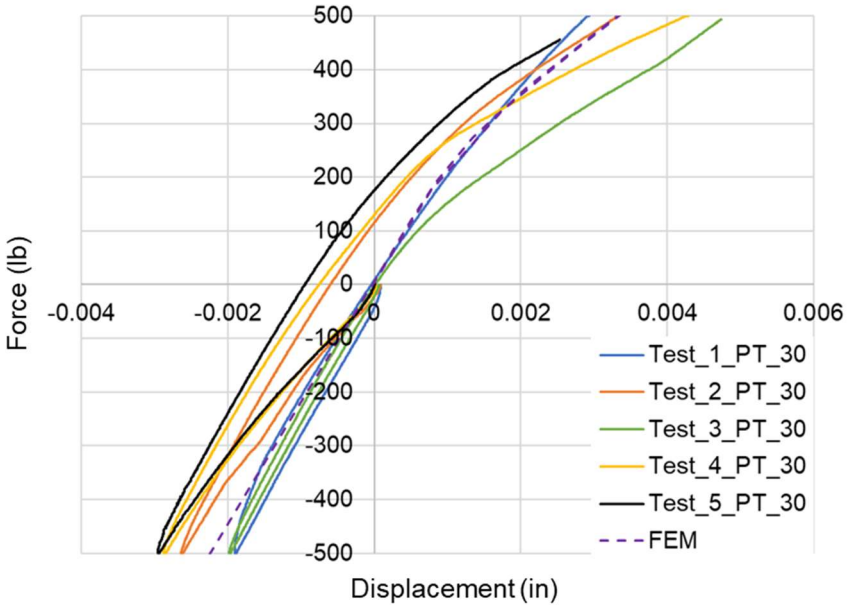

Figure 23. The test results and predicted load versus average measured displacement of axial test specimens with preload torque = 30 in-lb.

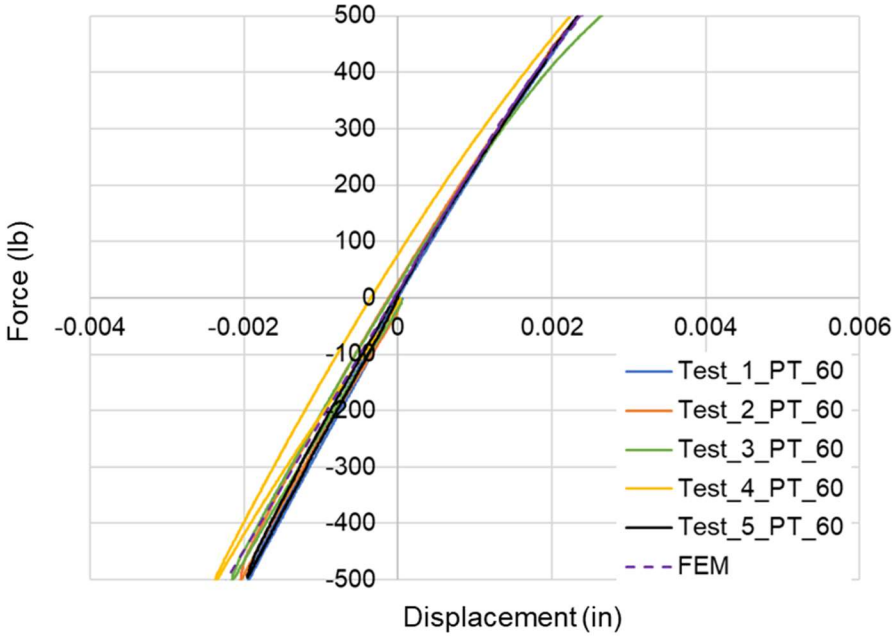

Figure 24. The test results and predicted load versus average measured displacement of axial test specimens with preload torque = 60 in-lb.

2.2.3 Equivalent Axial Stiffness of Multi-nut Joint

Equivalent axial stiffness (EA) of the multi-nut joint was calculated to be 1.697 x 10^6 lb. from the average test result slope (EA/L = ΔP/Δd) of the specimen load-displacement response curve, as shown in Figure 25.

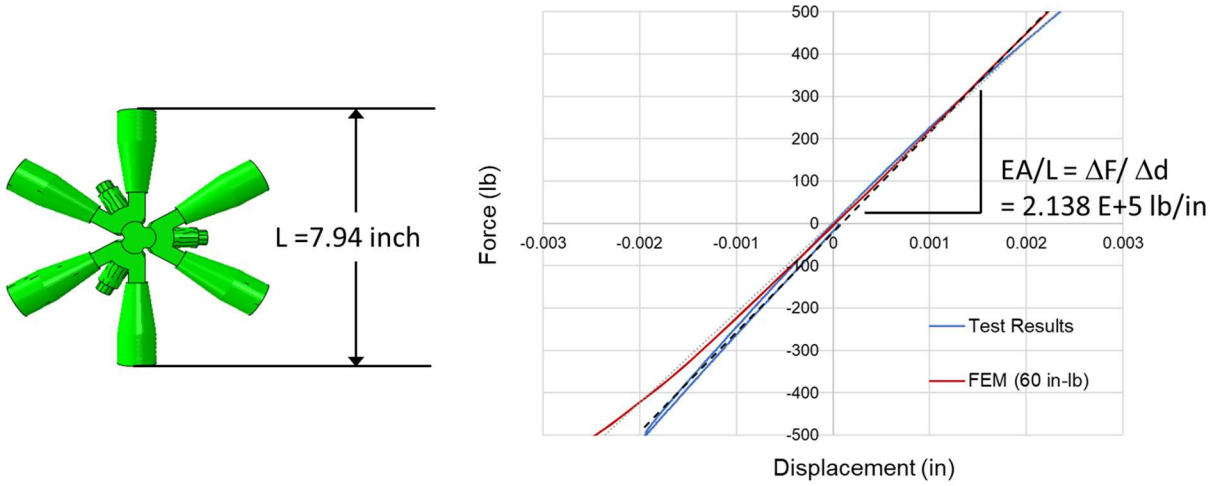

Figure 25. Axial stiffness of multi-nut joint.

2.2.4 Summary of the Axial Test

The axial tests for the multi-nut joint were performed and FEM of the axial test specimen was developed. Nonlinear static analysis of FEM was performed, and the FEM results were compared with test results. The summary of axial test and FEM are:

1. The test procedure was verified through the calibration specimen and the correlating closed form solutions and the FEM of the calibration specimen.
2. The fastener torque and the length of the fastener affect the linearity and repeatability of the joint axial load.
3. Increasing the fastener torque to the specs increased the tension linearity and repeatability in the load range.
4. Increasing the length of fastener also improved repeatability and linearity by engaging more threads.
5. Based on the test results, the installation preload fastener torque value and the length of fastener were obtained as 60 in-lb and 55 mm, respectively.
6. An equivalent axial stiffness of 2.138 x 10^5 lb/in was calculated for future analysis of assembled TriTruss structures within the ± 500 lb member load range and the 60 in-lb fastener torque.

3.0 Multi-Nut Joint Bending Test

The multi-nut joint bending test were conducted utilizing a three-point bend test setup, similar to the one described in Reference [7]. The objectives of the bending test were to:

1. Evaluate multi-nut joint performance bending stiffness performance and provide reference data.
2. Determine an equivalent EI of the multi-nut joint over the two corner nodes and multi-nut joint for different joint orientations.
3. Provide multi-nut joint bending performance results to validate the finite element model of multi-nut joint.

Bending test setup and calibration specimen, the modeling of a multi-nut bending test specimen, the bending test results and multi-nut performance, and the calculated equivalent bending stiffness of the multi-nut joint are provided in this section.

3.1 Bending Calibration Test and Analysis

As with the multi-nut equivalent axial stiffness test discussed in Section 2, a calibration specimen was used to develop and verify an equivalent bending stiffness test. The objective of the calibration test was to verify the bending test equipment, setup, and to provide reference data. The bending stiffness calibration tests were performed using an aluminum tube specimen. In addition, three composite tube specimens with manufacturer provided stiffness values were tested for verification of bending stiffness properties prior to the bending test of the multi-nut joint specimen. The composite tube data will be used with the results of the multi-joint bending test to calculate the equivalent EI of the multi-joint. All tests were performed at the room temperature. The details of aluminum calibration tube specimen and composite calibration test tube specimens are presented in Table 1.

Table 1. Tube specimen information.

Material	Aluminum	Composite
Length	6 feet	6 feet
Outer diameter	1.25 inch	1.195 inch
Inter diameter	1.12 inch	1.125 inch
Thickness	0.065 inch	0.035 inch
Elastic Modulus	1.00×10^7 psi	2.93×10^7 psi**

** Value provided by manufacturer.

For the three-point bending test, a tube specimen was rested on specially designed cradle fixtures representing simply supported end conditions. The fixtures were placed 6 inches from the end of the tubes to establish a simply supported boundary conditions. The design of the support cradle and simply support fixtures are shown using the fabrication drawing, Figure A-3 of Appendix A. Weight was suspended at the midpoint of the joint to apply the bending load. Displacements were measured using five LVDTs: one at the center of the test specimen, two 3.47 inches from the

center, and two at the simply supported boundary. The bending test setup and aluminum calibration tube are shown in Figure 26. A close-up view of the cradle and simply support fixture is shown in Figure 27.

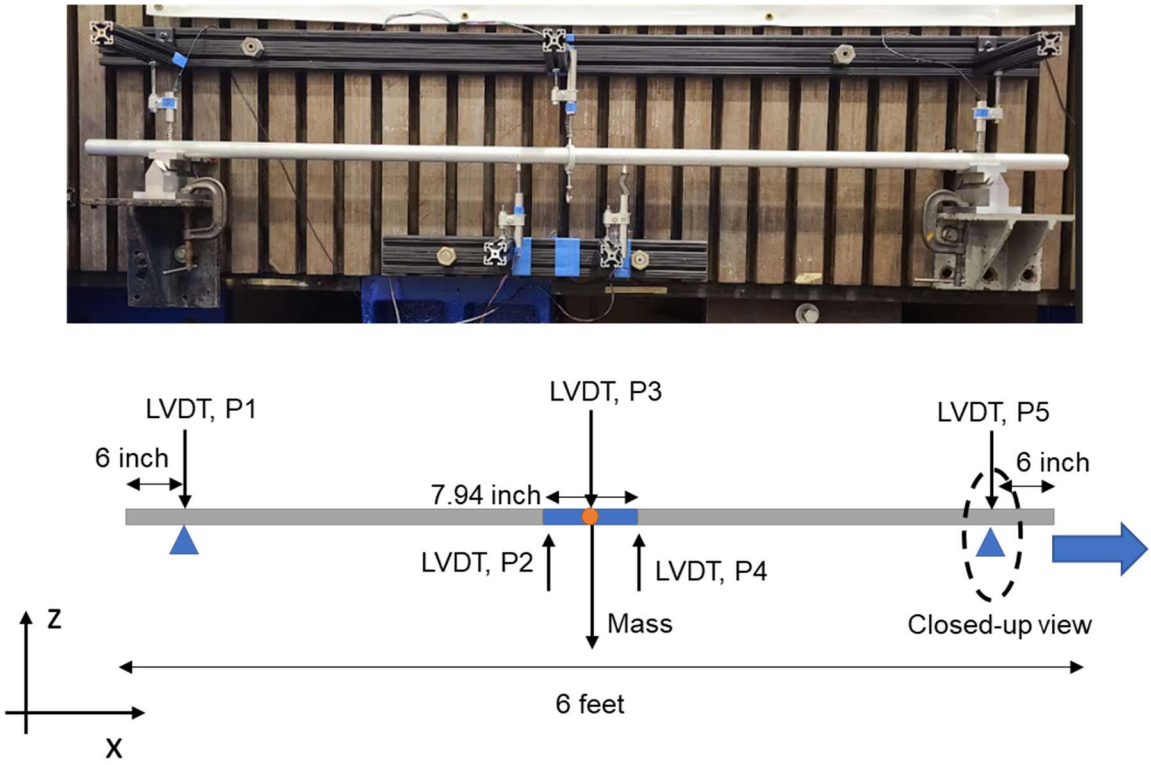

Figure 26. Bending test setup.

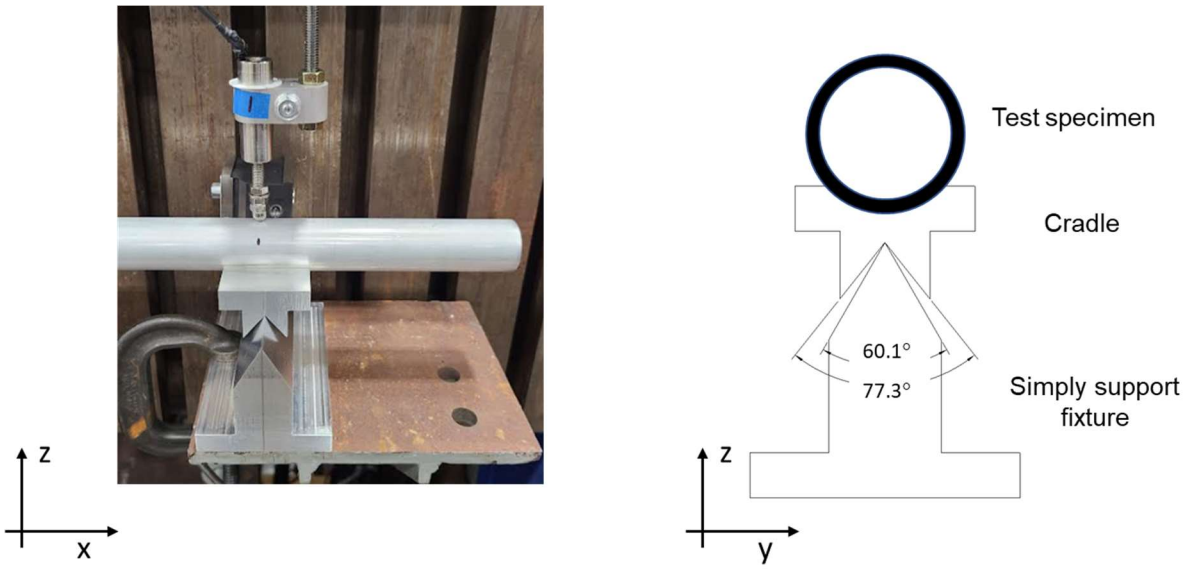

Figure 27. Close-up view of the cradle and simply support fixture.

The center displacement response due to the load provided the load-deflection response for characterization of the bending performance of the specimens.

3.1.1 Aluminum Specimen Tube Results

A three-point bending test was performed for the aluminum tube. Weights were incrementally added to the middle of the aluminum tube using a hanging fixture that had a weight of 3 lb. The applied test loads were 5 lb, 10 lb, 20 lb, 30 lb and 40 lb. Static analyses were performed on the FEM subjected to bending load. The load-deflection response of the aluminum calibration tube was compared with the predicted pretest analysis results and the closed-form solution. Figure 28 presents the test results, predicted pretest results, and the closed-form solution.

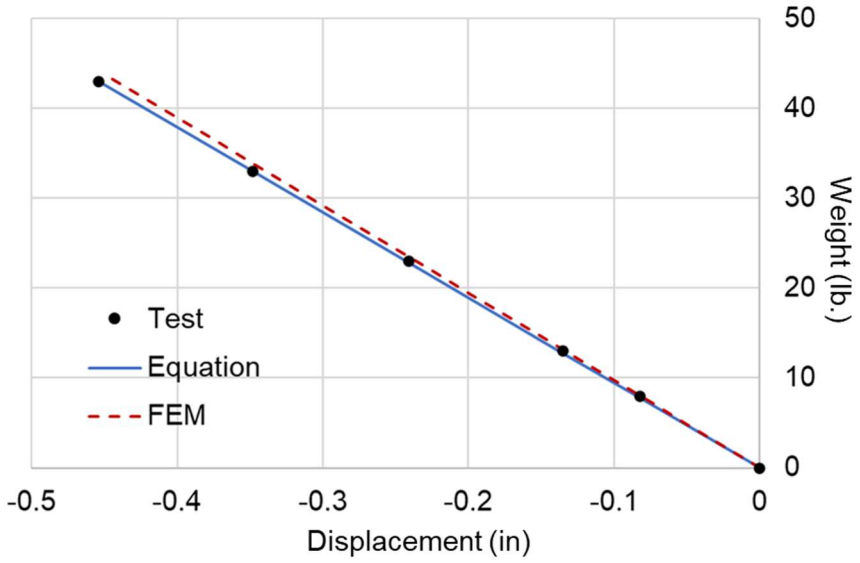

Figure 28. Load-deflection response of the aluminum calibration tube.

The comparison of results in Figure 28 shows that the test results were consistent with the pretest predictions and the closed-form solution. The test results were less than 1% different from pretest predictions and the closed-form solution, thus demonstrating the reliability of the bending test setup.

3.1.2 Composite Specimen Tube Results

Three-point bending tests were performed for three composite tubes. Weights were incrementally added to the middle of the composite tube using a hanging fixture that had a weight of 3 lb. The total applied load was 43 lb. including the weight of the hanging fixture with 5 lb. increment.

The load-deflection response of the three-point bending test on the composite tubes and the average of the test response are presented in Figure 29. Also, the load-deflection response of the composite tube was calculated using three different elastic moduli, the manufacturer provided modulus (E, 29 Msi), 20% reduced modulus (23 Msi), and 30% reduced modulus (20 Msi), and presented in Figure 29. The test results are in relatively good agreement, within +/- 5% of the average result. The calculated load-deflection response using the manufacturer provided modulus (29 Msi), shows stiffer than test results, while the calculated load-deflection response using 20%

reduced modulus was consistent with test data, as shown in Figure 29. The elastic modulus of the composite tube was previously determined through compression and tension modulus tests conducted by the PASS project; revealing values of 24 Msi for tension and 22 Msi for compression [9, 10]. These results indicate that the manufacturer provided modulus was inaccurate and the elastic modulus of the composite calibration tube was closed to 23 Msi (a 20 % reduction from the manufacturer provided modulus). The elastic modulus of 23 Msi was used in the FEM for the composite calibration tube.

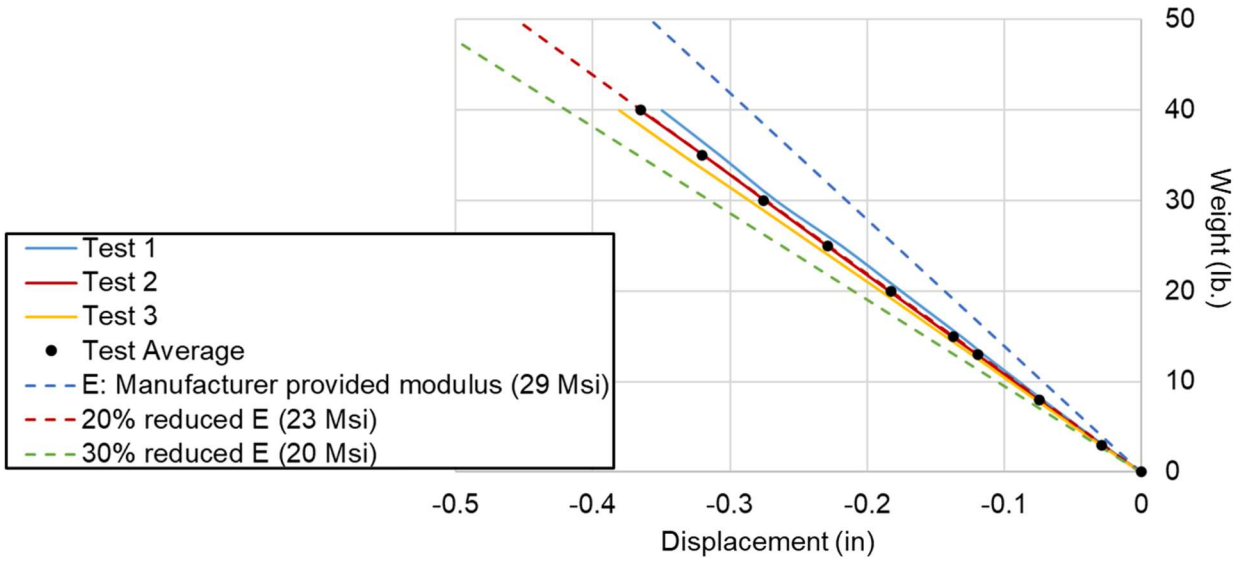

Figure 29. Load-bending response of composite calibration tubes.

Static analyses were performed on the FEM subjected to a bending load. The load-deflection responses of the composite tubes were compared with the predicted pretest analysis results and the closed-form solution. The comparison of results in Figure 30 shows that the test results correlated accurately with the pretest predictions and the closed-form solution (exhibiting a difference of less than 1% in the load-deflection response) and demonstrates the reliability of the bending test setup.

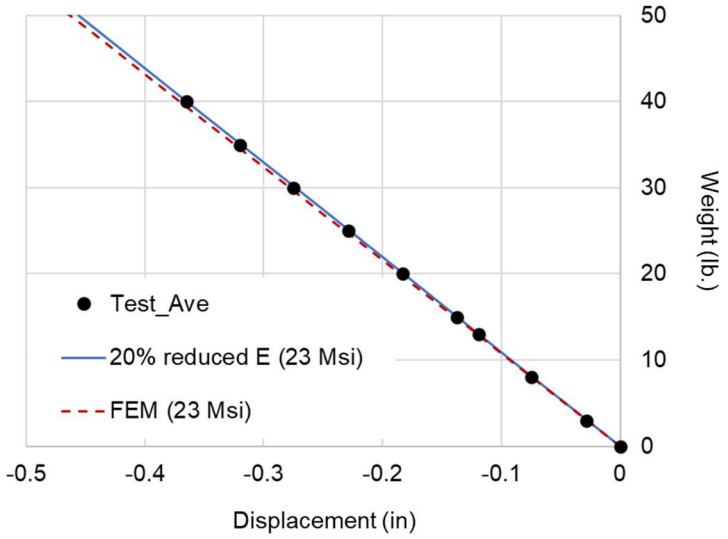

Figure 30. Test results and predicted load-bending response of composite calibration tubes.

3.2 Multi-Nut Bending Test and Analysis

Three 6-foot-long test specimens were fabricated for the multi-nut bending test. These specimens included a 7.94-inch-long joint section comprising three corner nodes and a multi-nut joint as shown in Figure 31.

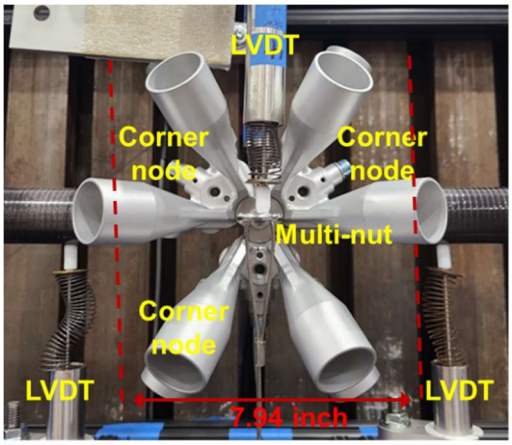

Figure 31. 7.94-inch-long joint section.

The multi-nut joint was evaluated for two preload values (60 in-lb and 120 in-lb). The test specimens were subjected to four different bending orientation as shown in Figure 32: downward, upward, side 1, and side 2 orientations. Figure 31 shows the multi-nut joint section with these four test orientations.

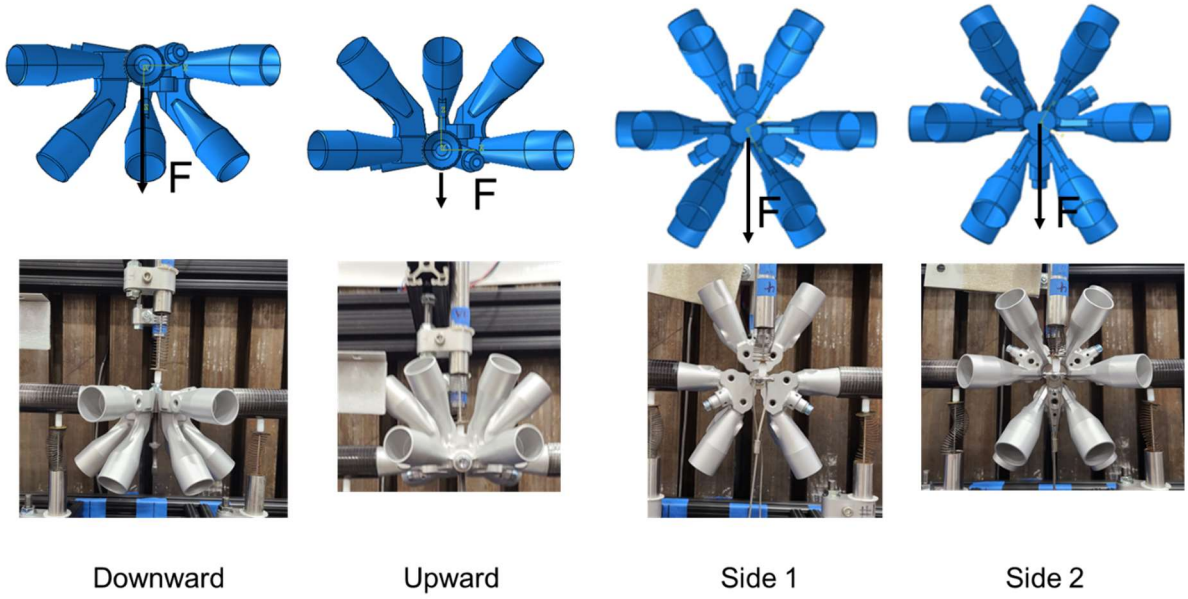

Figure 32. Bending test orientation.

For the downward and upward orientation, the applied weight was hung from a hanger attached to the bottom of a multi-nut joint. The mid-point deflection of the test specimen was measured at the top center of the multi-nut. In the cases of the side 1 and side 2 orientation, wing head screws were attached to both the bottom and top of the multi-nut joint. Steel rings were looped around the wing head screws and connected to the weight hanger. Subsequently, the applied weight was hung from the weight hanger, and two LVDTs measured deflections from the wing head screws. The deflection data from the two LVDTs was averaged to provide the joint overall deflection. The LVDT and weight hanger setup for side 1 orientation is presented in Figure 33.

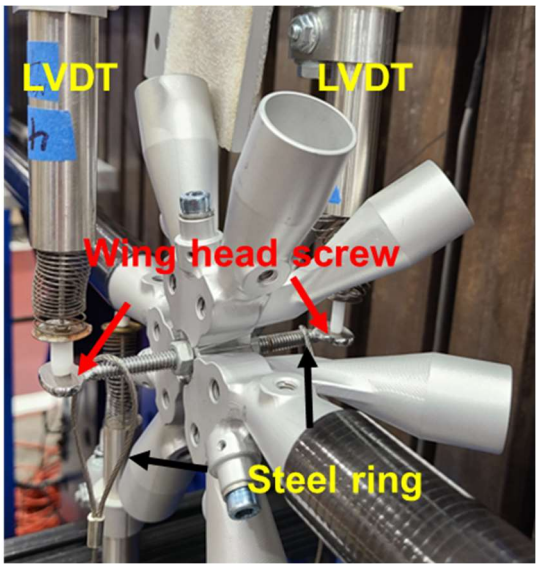

Figure 33. LVDT and weight hanger setup for side 1 orientation.

Table 2 lists three bending test specimens with the test configuration and corresponding fastener torque. The detailed bending test procedure of the bending test specimen is described in Appendix B.

Table 2. The test specimen configurations and fastener torque.

Configuration	Up	Down	Side 1	Side 2
Specimen 1				
Fastener load 60-in-lb	√	√	√	√
Fastener load 120-in-lb	√	√	√	√
Specimen 2				
Fastener load 60-in-lb	√	√	√	√
Fastener load 120-in-lb	√	√	√	√
Specimen 3				
Fastener load 60-in-lb	√	√	√	√
Fastener load 120-in-lb	√	√	√	√

(Check mark indicate the completion of test)

3.2.1 Multi-Nut Bending Test Results

In this section, the load-deflection response of the bending test specimens for different loading orientations and preload torque values are presented and discussed. For each test specimen, the load was applied to the test specimen until the deflection reached closed to 1 inch. Load-deflection responses of the test specimens with preload torques of 60 in-lb and 120 in-lb for different loading orientations are shown in Figures 34 through 37. In these figures, solid lines represent the load-deflection responses of the test specimens with the preload torque of 60 in-lb and dash lines represent the load-deflection responses of the test specimens with the preload torque of 120 in-lb.

The load-deflection responses for the test specimens in the downward orientation are presented in Figure 34. All test specimens exhibited an initial linear load-deflection response. As the load was increased, existing gap between the multi-nut and fasteners, as well as the interface between corner nodes and the multi-nut, closed and interlocked. Consequently, the load-deflection responses of the test specimens changed from the initial linear slope to a nonlinear slope as the physical gaps were closed. Then the slopes began to resume a linear slope after the gaps were presumed closed and interlocked. As seen in Figure 34, the slopes of the test specimens with the preload torque of 120 in-lb exhibited a stiffer slope, compared to the test specimens with the preload torque of 60 in-lb. In the case of the test specimens with the preload torque of 60 in-lb the change from a linear to non-linear response occurred at the applied load of 15 lb. On the other hand, for the test specimens with the preload torque of 120 in-lb, the change from a linear to non-linear response occurred at the applied load of 20 lb.

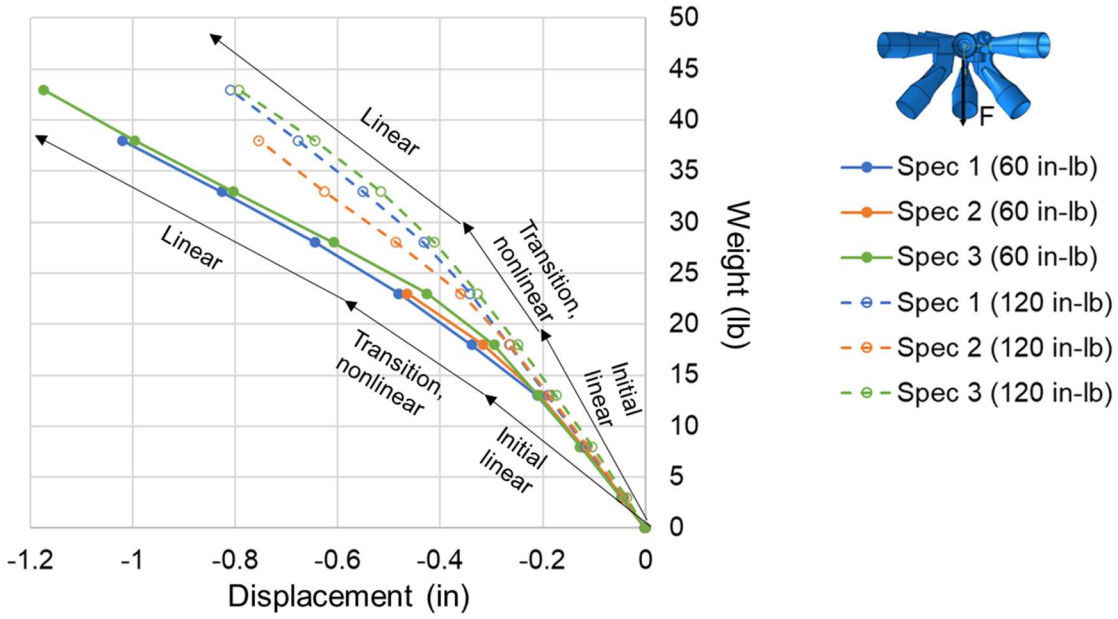

Figure 34. Load-deflection responses of test specimens, downward orientation.

The load-deflection responses of the test specimens in the upward orientation are presented in Figure 35. Similar to the load-deflection responses of the test specimens in the downward orientation, all test specimens in the upward orientation exhibited an initial linear load-deflection response which then transformed to a nonlinear slope followed by a return to a linear slope response. As seen in Figure 45, the higher preload torque value, resulted in a stiffer load-deflection slope.

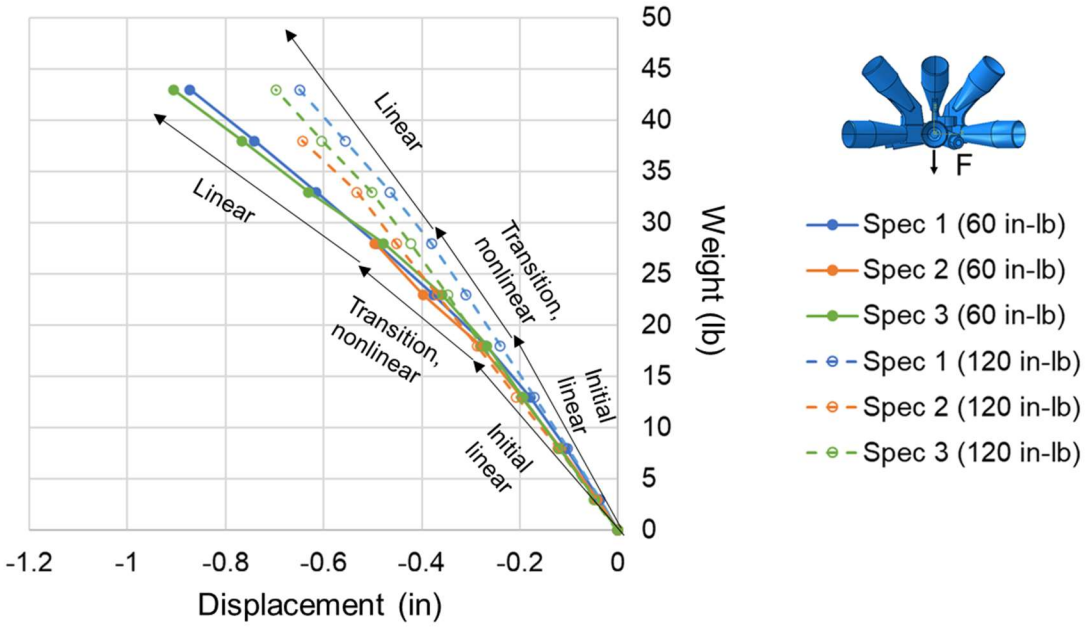

Figure 35. Load-deflection responses of test specimens, upward orientation.

The load-deflection responses of the test specimens in the side 1 and 2 orientation are presented in Figure 36 and 37, respectively. All test specimens subjected to the side 1 and 2 orientations exhibited an initial linear load-deflection response which then transformed into a nonlinear response. The test specimens with the preload torque of 120 in-lb consistently transitioned at a higher load than the specimens with the preload torque of 60 in-lb.

After each test specimen under different orientations, the test specimens were reconfigured to remove the deformed shape from the previous bending test, since the specimens physically realigned under load as indicated by the change in slopes, as well as could be visibly witnessed. In Figure 36, the load-deflection response of the test specimen 1 with the preload torque of 60 in-lb was significantly stiffer than other two test specimens with the preload torque of 60 in-lb. The stiffer response is suspected to result from the test specimen 1 not having been properly aligned prior to the side 1 loading profile, after the specimen had gone through a previous load test.

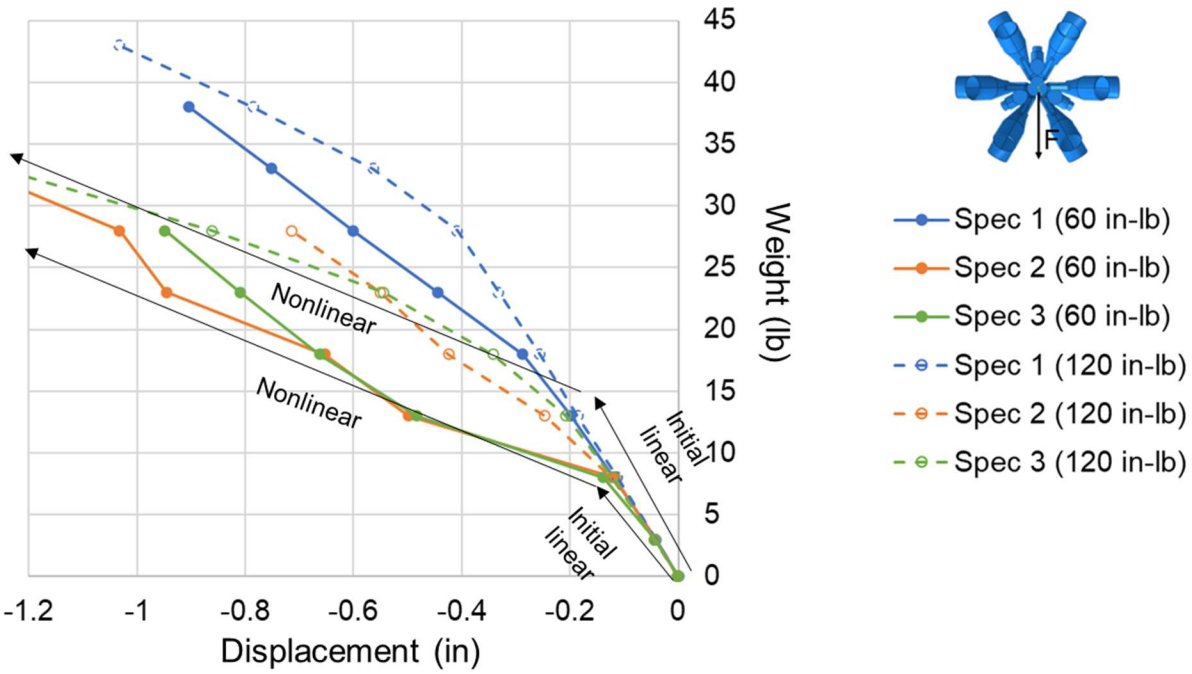

Figure 36. Load-bending responses of test specimens under side 1 orientation.

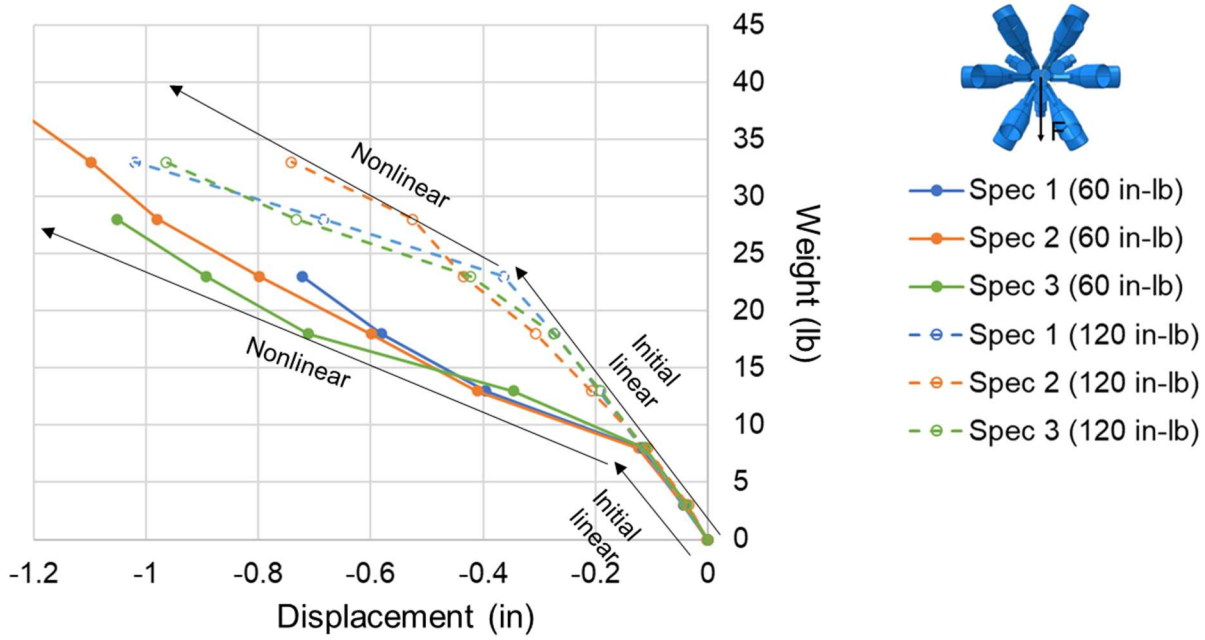

Figure 37. Load-bending responses of test specimens under side 2 orientation.

The load-deflection response of the test specimens with different preload torque are presented in Figures 38 through 40. As it can be seen in the figures the load-deflection stiffness response of the multi-nut joint is nonlinear likely due to the clearance gaps between fasteners and multi-nut, and the complex geometry in the interface between corner nodes and the multi-nut surface. The initial assembly conditions and complex geometry could cause the inconsistent nonlinear response of the test specimens and difference in the maximum applied load required for one-inch center deflection of the test specimens. The load-deflection response for the up and down configurations is similar as is the response for the side 1 and side 2 configurations. The up and down configurations appear to have a stiffer response than the side 1 and side 2 configurations for any given specimen. As also demonstrated in the axial stiffness test results, the higher fastener load supports a stiffer response and a smoother transition from a linear to non-linear curve as the applied load increases.

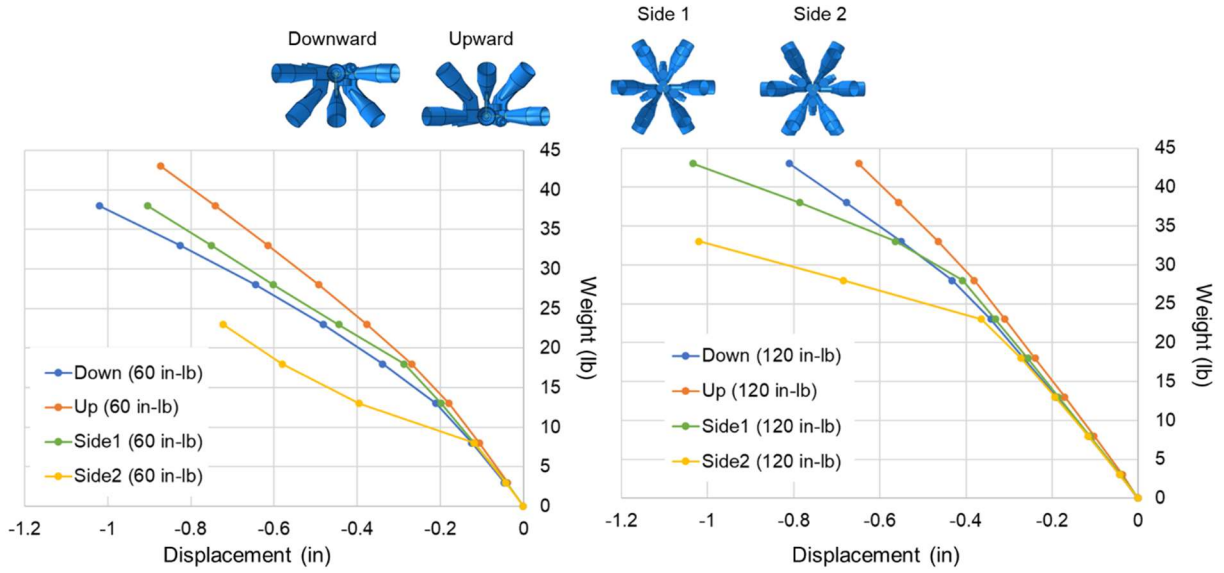

a) Preload torque 60 in-lb

n) Preload torque 120 in-lb

Figure 38. Load-bending response of test specimen #1

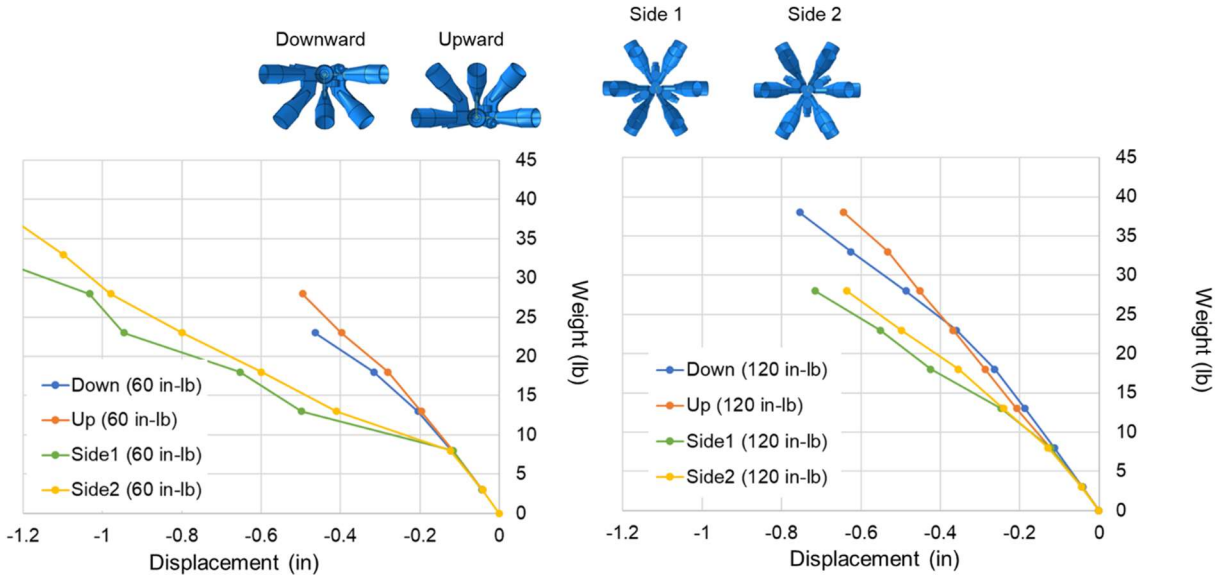

a) Preload torque 60 in-lb

n) Preload torque 120 in-lb

Figure 39 Load-bending response of test specimen #2

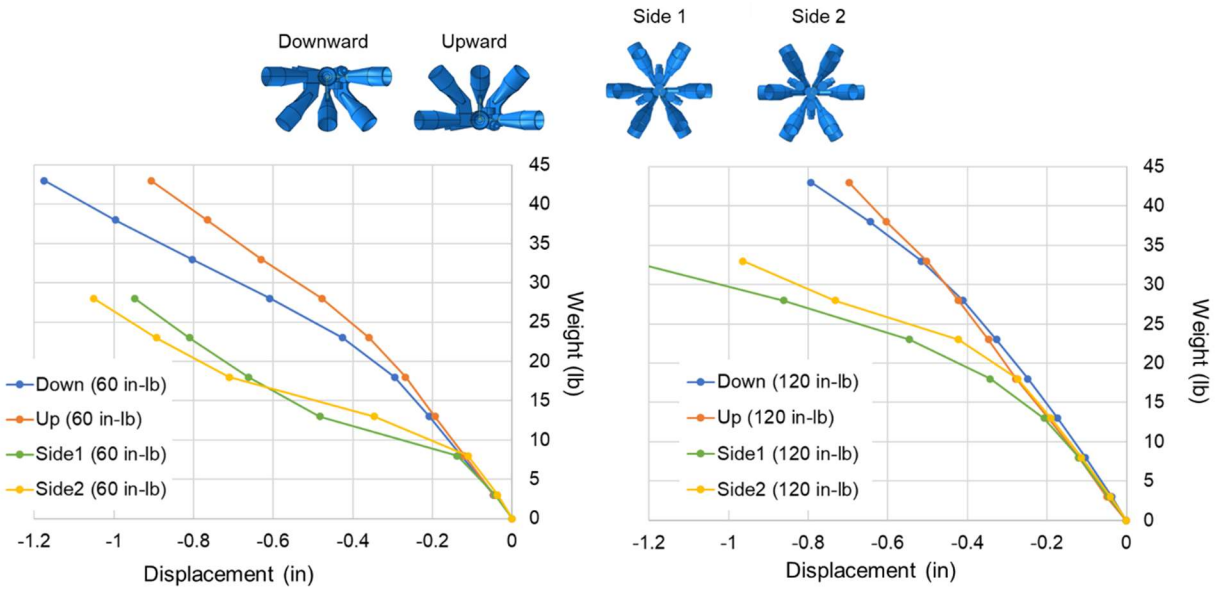

a) Preload torque 60 in-lb

n) Preload torque 120 in-lb

Figure 40. Load-bending response of test specimen #3

3.2.2 Finite Element Models of the Bending Test Specimen

For test-analysis comparisons, a FEM of the bending test specimen was developed using Abaqus eight-node linear brick element with reduced integration (C3D8R) and ten-node tetrahedral element (C3D10) elements [6]. The total number of nodes is 223420 and total number of elements is 129900. The isotropic modulus of elasticity of 30 x 10^6 psi and Poisson ratio of 0.3 were used for nodes and multi-nut of the FEM. The isotropic modulus of elasticity of 23 x 10^6 psi and Poisson ratio of 0.3 were estimated from the composite tube specimen test and used for the FEM of composite tube. Fasteners were modeled with two Abaqus general Timoshenko beam elements (B31). Both ends of the fasteners were attached via kinematic constraints to the multi-nut and the corner node and the preloaded torque was applied to the middle-connected node of beam elements. The contact constraints were applied to the interfaces between the multi-nut and corner nodes. Fastener modeling with contact conditions and beam elements are presented in Figure 41.

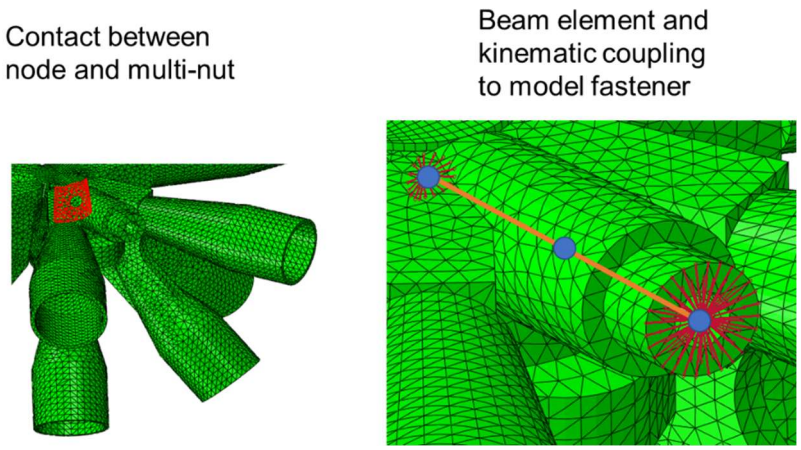

Figure 41. Fastener Modeling with Contact Condition and Beam Elements.

Four different bending orientations were applied to the FEM of the bending test specimen using different displacement constraint conditions at the simply supported locations. Boundary and loading conditions of the FEM for the bending test specimen for downward and side 2 orientations are shown in Figure 42.

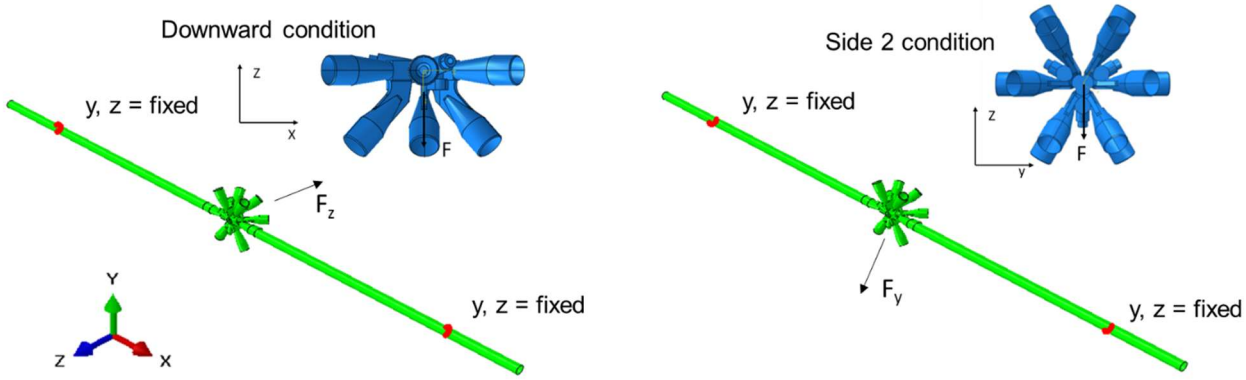

Figure 42. Boundary Condition of Finite Element Model of the Bending Test Specimen.

The predicted load-deflection responses of FEMs under downward and upward orientations are presented in Figures 43. In Figure 43, blue curves represent the predicted results of downward orientation, orange curves represent the predicted results of upward orientation, solid curves represent the FEM with preload torque of 60 in-lb and dotted curves represent the FEM with preload torque of 120 in-lb. Similar to the test results, an initial linear load-deflection response was exhibited by all predicted load-deflection responses of the FEM. As load was applied, an interlocked condition was simulated to represent the closing of the interface between corner nodes and multi-nut assembled conditions. The gaps in the fastener and the multi-nut could not be simulated since the fastener was modeled with beam elements. Consequently, a change in the slope of the load-deflection responses of the FEM was observed when the interlocked condition was reached. The predicted load-deflection responses of FEMs indicated that the load-deflection

responses of FEMs with upward orientation were stiffer than the load-bending responses of FEMs with downward orientation. The effect of the higher preloaded torque of the fasteners was emulated by developing the interlocked condition with the application of more load.

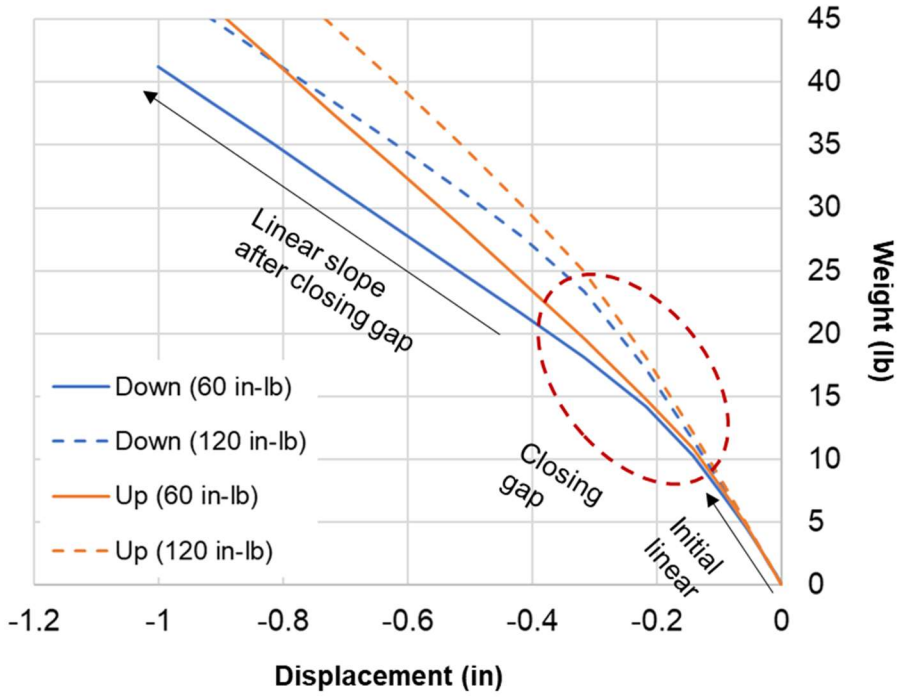

Figure 43. Load-deflection responses of FEM in downward and up orientation.

Comparisons between the predicted load-deflection response from FEMs with 60 in-lb and 120 in-lb preload torque and the test results for downward orientation are shown in Figure 44 and 45 and for upward orientation in Figure 46 and 47. Comparisons between the predicted load-bending response from the FEM and the test results indicated that the predicted response of the FEM were consistent with the test results for both downward and upward orientation.

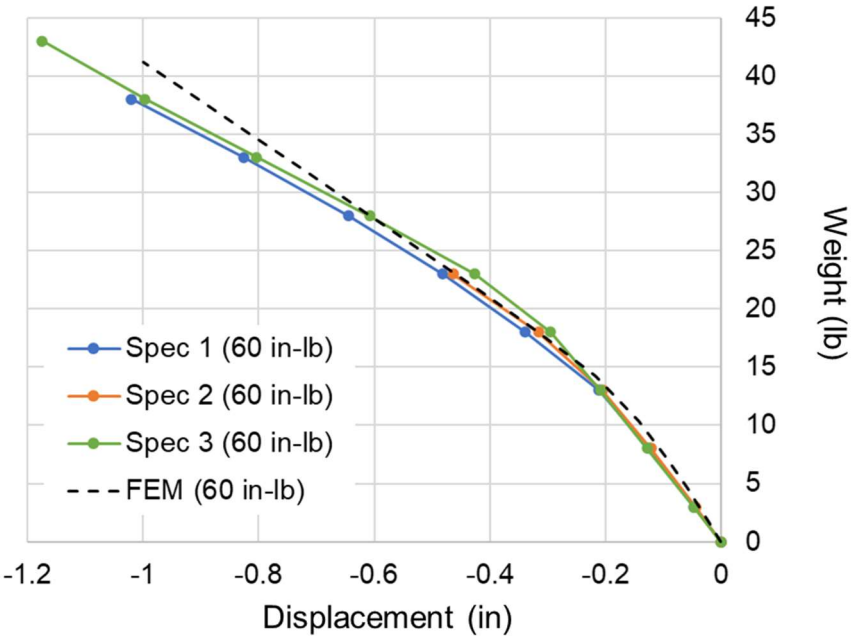

Figure 44. The test results and predicted load-deflection response of test specimens (Downward orientation, preload torque = 60 in-lb).

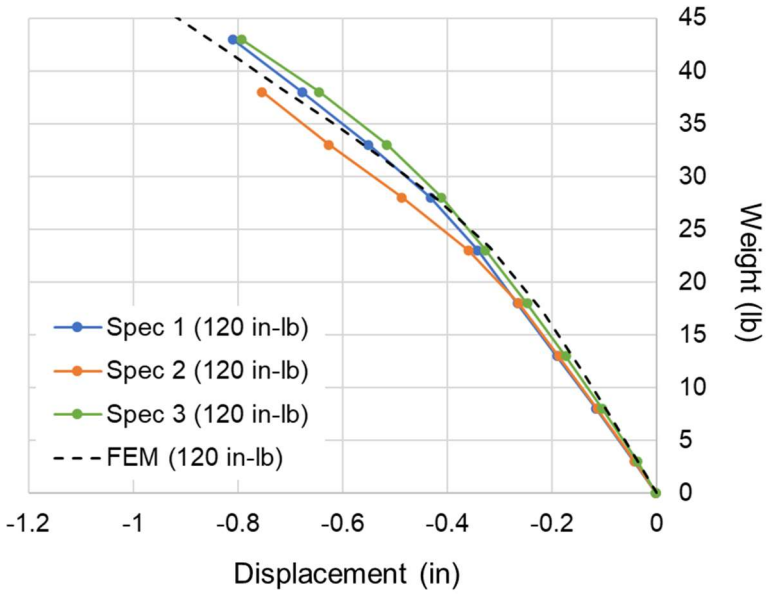

Figure 45 The test results and predicted load-deflection response of test specimens (Downward orientation, preload torque = 120 in-lb).

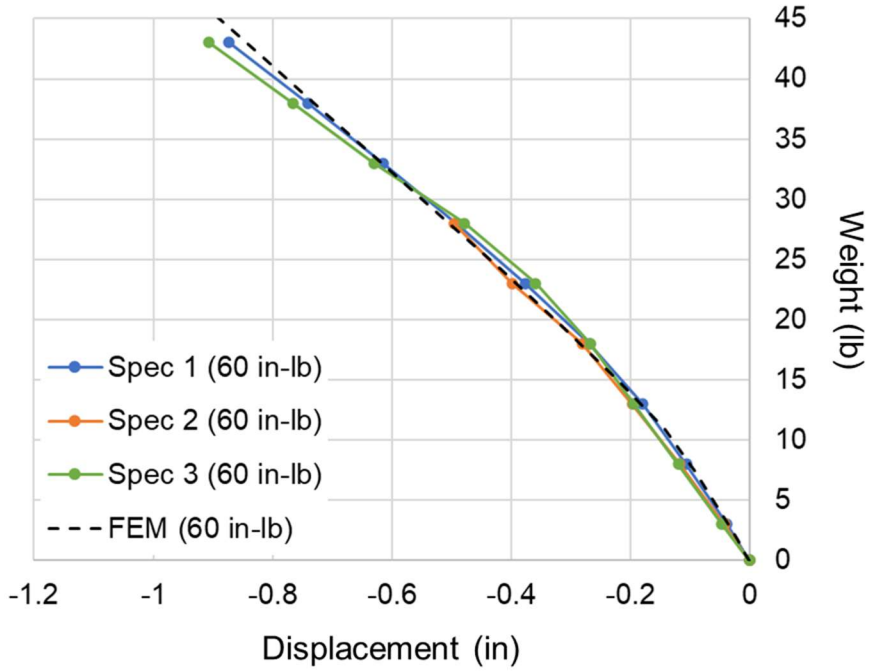

Figure 46. The test results and predicted load-deflection response of test specimens (Upward orientation, preload torque = 60 in-lb).

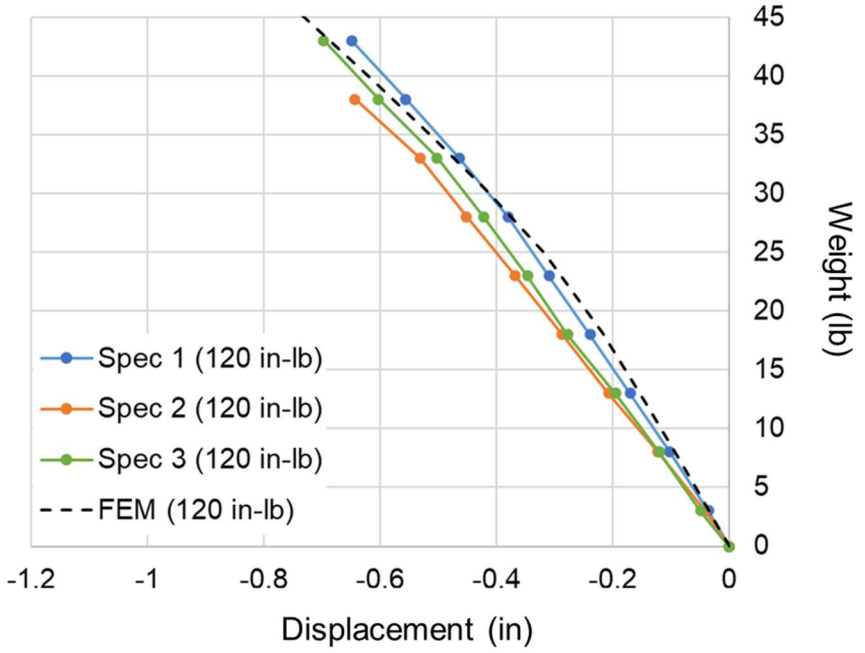

Figure 47. The test results and predicted load-deflection response of test specimens (Upward orientation, preload torque = 120 in-lb).

The predicted load-deflection responses of FEMs for side 1 and side 2 orientation are presented in Figures 48. For both side 1 and side 2 orientations, the linear load-deflection responses of the test specimens were predicted from FEMs. The interaction between the corner nodes and the multi-nut was not simulated from FEMs.

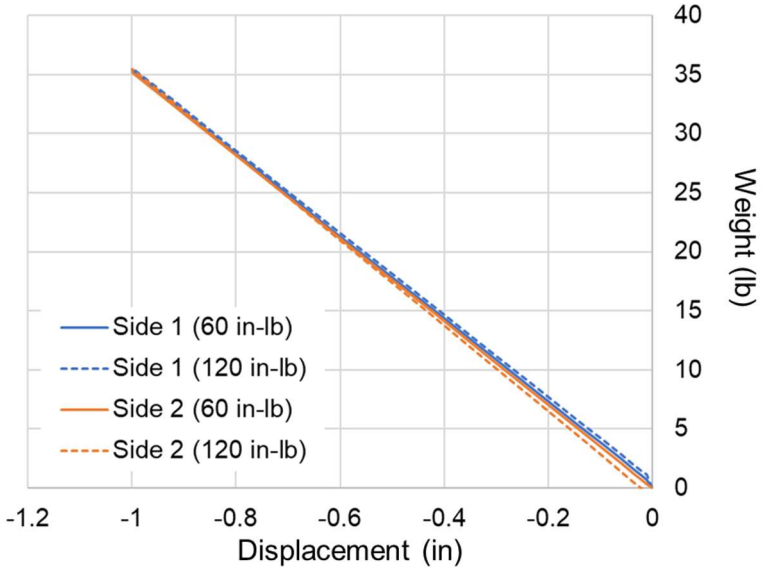

Figure 48. Load-deflection responses of FEMs for side 1 orientation.

Test-analysis comparisons indicated that FEMs of the test specimen were not able to predict the load-deflection response consistent with test results due to lack of modeling details around the interface between fasteners, the multi-nut, and nodes. Fasteners in the multi-nut joints were modeled with beam elements but the clearance between fasteners and the multi-nut was not included in the FEM. Also, the complex geometry in the interface between corner nodes and multi-nut surfaces was not properly modeled in FEMs of the multi-nut joint. Sensitivity analysis of the friction on the interface between the corner node and multi-nut joint was performed to add interaction between nodes and the multi-nut joint. For the sensitivity analysis, three different friction parameters, 0.07, 0.15, and 0.3, were added in the contact constraint between the nodes and multi-nut surfaces.

Test-analysis results of load-deflection response of the test specimens with preloaded torque of 60 in-lb and 120 in-lb for side 1 orientation were shown in Figures 49 and 50, respectively. In Figures 49 and 50, solid lines represent the test results, while dotted lines represent the predicted load-deflection response of FEMs with different friction parameters. The predicted load-deflection responses of FEMs with friction parameters showed the initial linear response and predicted the interlocked condition as load was applied. An increase in the friction parameter of the FEMs results in the interlock condition occurring at a higher applied load. Although FEMs weren't able to predict the slope of the load-deflection response and nonlinear response from the interlock condition of the test specimens, for both FEMs with preload torque 60 in-lb and 120 in-lb, the FEM with the friction parameter of 0.15 simulated the interlock condition and showed similar trends of the load-deflection response with the test results.

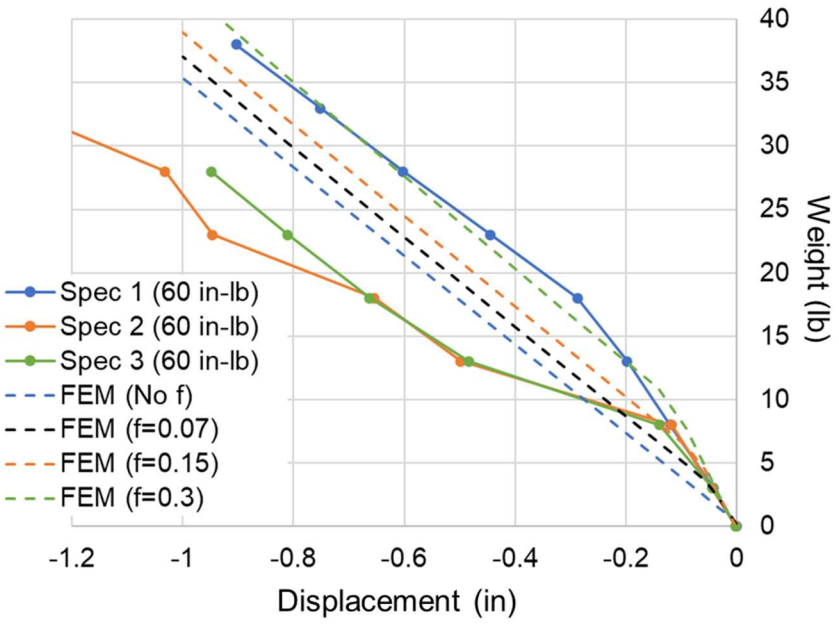

Figure 49. Test and analysis results of FEMs with different friction parameter for side 1 orientation (Preload torque = 60 in-lb).

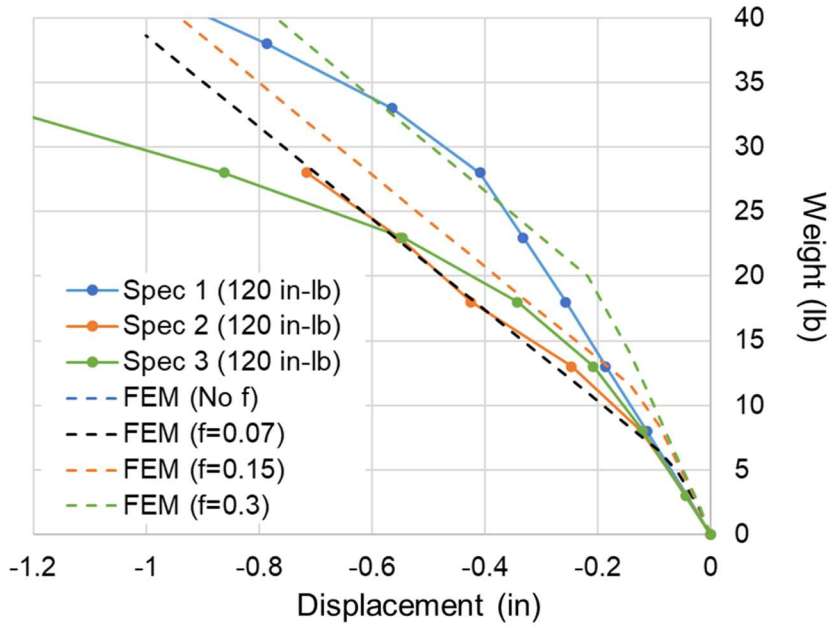

Figure 50. Test and analysis results of FEMs with different friction parameter for side 1 orientation (Preload torque = 120 in-lb).

Test-analysis results of load-deflection response of the test specimens with preloaded torque of 60 in-lb and 120 in-lb for side 2 orientation were shown in Figures 51 and 52, respectively. In Figures 51 and 52, solid lines represent the test results, while dotted lines represent the predicted load-deflection response of FEMs with different friction parameters. Similar to the predicted linear load-deflection response of FEM for side 1 orientation, FEMs with friction parameters predicted the initial load-bending response and interlock condition with the friction parameter of 0.15. However, after the interlock condition was reached, the load-deflection responses of FEMs were not consistent with test results. Including clearance between fasteners and the multi-nut utilizing gap element or connect elements and more detailed features in the interface and gap between nodes and the multi-nut are needed in the FEM to better simulate the load-bending response of the bending test specimen beyond the interlock condition.

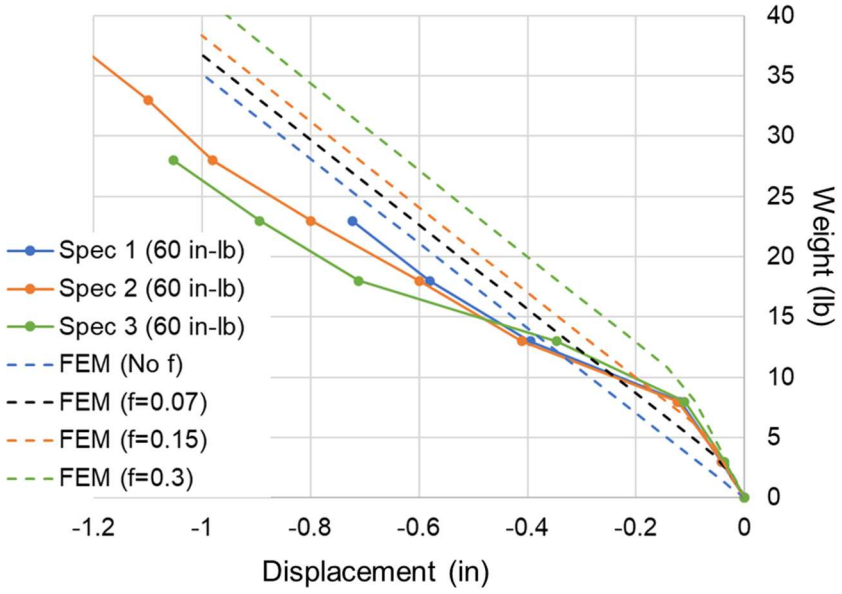

Figure 51. Test and analysis results of FEMs with different friction parameter for side 2 orientation (Preload torque = 60 in-lb).

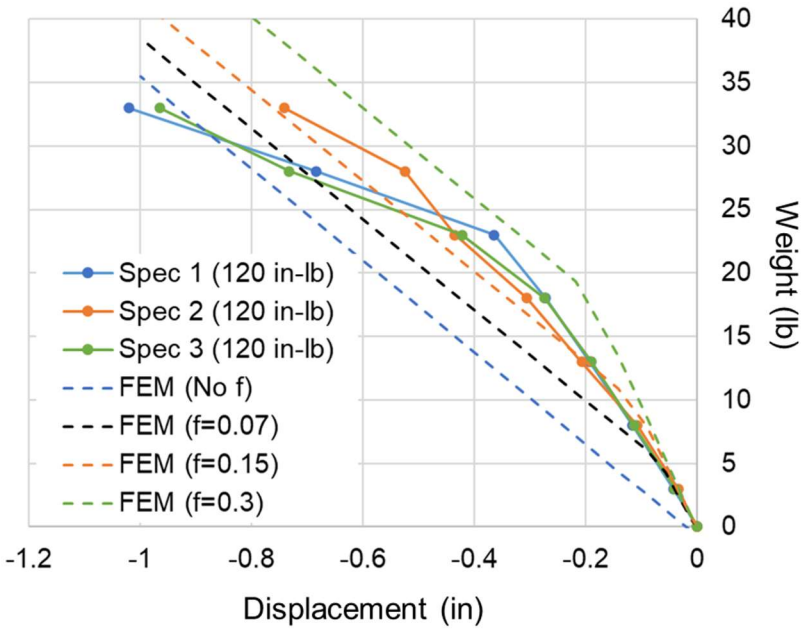

Figure 52. Test and analysis results of FEMs with different friction parameter for side 2 orientation (Preload torque = 120 in-lb).

3.2.3 Equivalent Bending Stiffness of Multi-nut joint

The equivalent bending stiffness of the multi-nut joint with the preload torque of 60 in-lb was calculated by Equation 1

$$EI_J = \left(\frac{L^3}{48} - \frac{a^3}{6}\right) \div \left(\frac{y}{P} - \frac{a^3}{6EI_s}\right), \quad (1)$$

where L is the distance between support, a is the distance from the support to the joint-node interface, y is the center deflection, and EI_s is the equivalent bending stiffness of the composite strut [7].

The equivalent bending stiffness of three multi-nut joints was computed. Then, the average equivalent bending stiffness of three multi-nut joints was normalized by the composite strut bending stiffness and was plotted against the corresponding loads for the bending orientation in Figure 53. The equivalent bending stiffness of the multi-nut was found to vary significantly for given bending orientations. As shown in Figure 53, the plot of the normalized stiffness decreases as the load is increased. For side 1 and side 2 configurations, the normalized stiffness reaches a constant value, while for the up and down configurations the normalized stiffness appears to trend toward an asymptote.

Among the four different bending orientations, the upward orientation results show a stiffer equivalent bending stiffness (22 % of the bending stiffness of the composite strut with 0.9 mid-deflection). For downward and upward orientations, the response is a nonlinear decrease of the equivalent bending stiffness. This represents the change in interaction between the corner nodes

and multi-nut surface from an initial assembly condition to an interlock condition. Equivalent bending stiffness of side 1 and side 2 orientations show the sudden drop of the equivalent bending stiffness and converges to 12 % of the bending stiffness of the composite strut. The drop of the bending stiffness for side 1 and side 2 orientation is due to slip along the interface between nodes and the multi-nut surface. The minimum equivalent bending stiffness values of the multi-nut joint for different bending orientation are summarized in Table 3. Based on the minimum bending stiffness and the load-deflection response for different bending orientation, the bending behavior of the multi-nut joint could be modeled and analyzed utilizing a torsion spring and other connector elements.

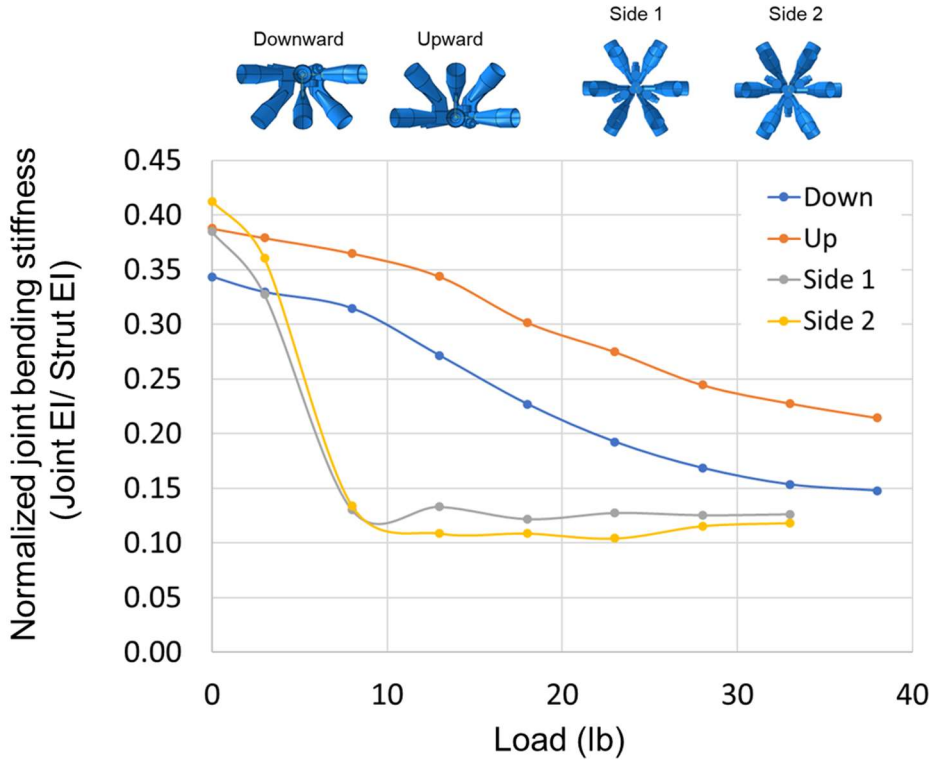

Figure 53. Normalized joint equivalent bending stiffness.

Table 3. Minimum equivalent bending stiffness of multi-nut joint in different bending orientation.

Orientation	Bending Stiffness (lb-in^2)
Downward	7.303×10^4
Upward	1.059×10^4
Side 1	6.237×10^4
Side 2	5.845×10^4

3.2.4 Summary of the Bending Test

The bending test setup of the multi-nut joint was established based on the calibration test. The bending test setup, as described in this report, allowed for precise measurement of the mid-deflection of the test specimen under various bending load orientations, enabling the calculation of the equivalent bending stiffness (EI) of the multi-nut joint based on the load-deflection response results. For all four different bending orientations, the load-deflection response of the multi-nut joint remained linear from the initial condition until the interlock condition was reached. However, as the bending load increased beyond the interlock condition, a nonlinear response was observed due to the complex geometry of the interlock condition at the node and multi-nut interface. In the case of side 1 and side 2 bending orientations, there was slippage between the multi-nut and nodes before reaching the interlock condition. These results also suggest that increasing the preloaded torque to the multi-nut joint increased the bending linearity and affects nonlinear response of the multi-nut joint. For example, the load-deflection responses of the multi-nut joint with the preloaded torque of 120 in-lb showed more linear and less nonlinear response than the load-deflection responses of the multi-nut joint with the preloaded torque of 60 in-lb.

The intricate nonlinear bending response of the multi-nut joint could not be adequately modeled using standard beam elements. Based on the observations from the bending test and the calculated minimum bending stiffness for different bending orientations, further modeling efforts are needed to simulate the bending response of the multi-nut joints. This may involve the incorporation of other connector elements such as gap and torsional spring elements to accurately capture the complex bending behavior of the multi-nut joint.

4.0 Summary

This report provides the details of the axial and bending tests conducted on a multi-nut joint. It includes axial and bending test results of the multi-nut joint. The axial test results provide insights into the installation preloaded torque value of the fastener. Additionally, the report presents sensitivity study of the impact of fastener length and clearance inside the multi-nut on the load-displacement response.

The bending test results examined the influence of bending orientation on the load-deflection response of the multi-nut joint. Based on the test results, EA and equivalent bending stiffness EI of the multi-nut joint have been estimated and are listed in Table 3. The test setup and procedures established in this study can be applied to assess equivalent EA and equivalent EI for other multi-nut joints. The report also provides modeling assumptions and approaches of FEM to predict the axial and bending response of the multi-nut joint. A comparison between the axial test and FEM analysis reveals that the predicted load-displacement responses from FEM align with the test results for FEMs with preload torques of 60 in-lb and 120 in-lb. In the case of the bending test, FEM effectively simulated the initial linear load-deflection response from the assembled condition to the interlock condition. However, the report acknowledges the limitations of FEM in simulating the nonlinear response beyond the interlock condition, highlighting deficiencies in geometry details and the ability to model the interaction between nodes and the multi-nut. Suggestions for further modeling approaches are proposed to address these limitations.

5.0 References

[1] Cline, J., Simmons, L., Song, K., White, B., McGlothin, G., Dorsey, J.T. and Doggett, W.R., "TriTruss Packaging and Deployment Trade Study," 2020 AIAA Ascend Conference, AIAA 2020-4128, virtual,16-18 November 2020.

[2] Doggett, W.R., Dorsey, J.T., Jones, T., Mikulas, M., Teter, J.E., and Paddock, D. "TriTruss: A New and Novel Structural Concept Enabling Modular Space Telescopes and Space Platforms," 70th International Astronautical Congress, Washington DC, 21-25 October 2019.

[3] Mukherjee, R., Siegler, N., and Thronson, H., "The Future of Space Astronomy will be Built: Results from the In-Space Astronomical Telescope (iSAT) Assembly Design Study," 70th International Astronautical Congress, Washington DC, 21-25 October 2019.

[4] Song, K., Simmons, L., and Cline, J.E., "Modeling Effort of TriTruss Modular Structure for In-Space Assembled Telescope Foundational Structure," AIAA SciTech 2022 Forum, AIAA Paper 2022-0844, San Diego, CA & Virtual, 3-7 January 2022.

[5] White, B.W., Doggett, W.R., Dorsey, J.T., and Song, K., "Tessellation and Numerical Simulation of the iSAT Reflector," 2020 AIAA Ascend Conference, AIAA 2020-4192, virtual,16-18 November 2020.

[6] Dorsey, J.T., and Watson, T.T., "Summary of LaRC 2-inch Erectable Joint Hardware Heritage Test Data," NASA TM-2016-219189, March 2016.

[7] Wu, K.C., "Characterization of the Bending Stiffness of Large Space Structure Joints," NASA TM-101565, May 1989.

[8] Anon., ABAQUS™ 2021 Analysis User's Guide, Vols. I-V, Version 2021. Dassault Systèmes, Providence, RI, 2021.

[9] Simmons, L., and Song, K., "Testing of Bonds in a TriTruss Modul," 2023 AIAA SciTech Forum, National Harbor, MD, 23-27 January 2023,

[10] Simmons, L., "Elastic Modulus Testing for TriTruss Struts," NASA/TM–20230011547, October 2023.

6.0 Appendix

A. Support Drawings

Figure A-1. The axial calibration test specimen

Figure A-2. The thread adapter

Figure A-3. Support cradle and simply support fixtures

B. Bending Test Procedure

Figure A-1. The axial calibration test specimen

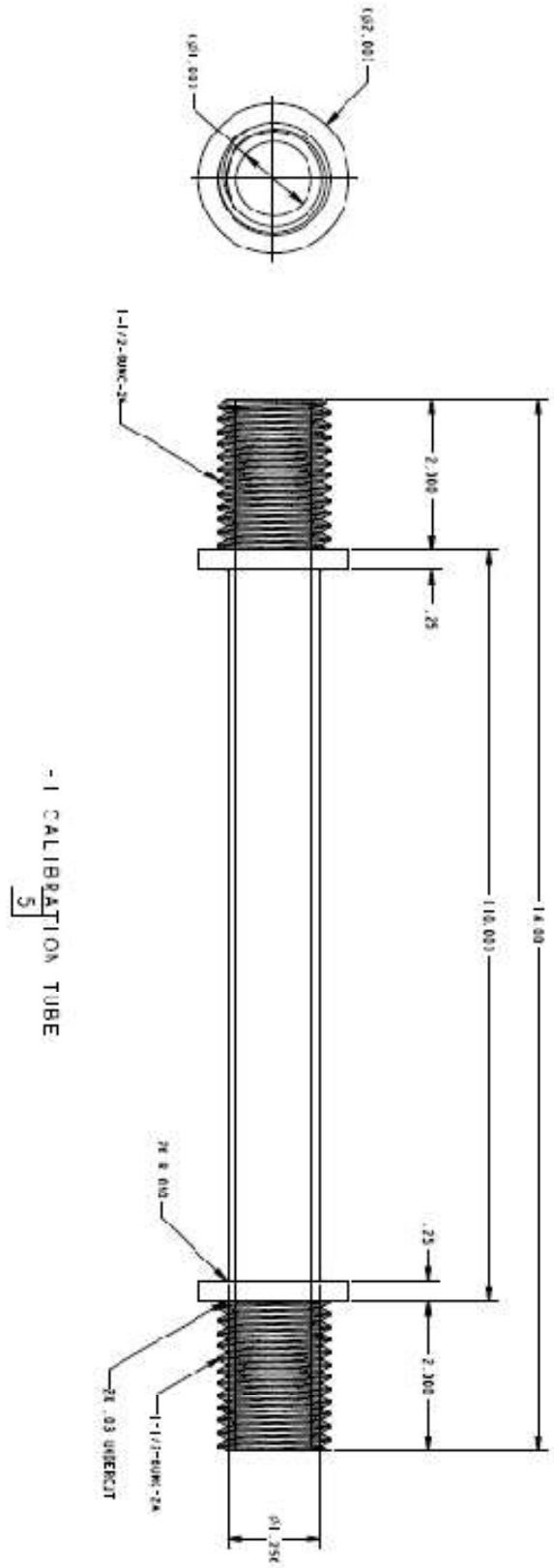

Figure A-2. The thread adapter

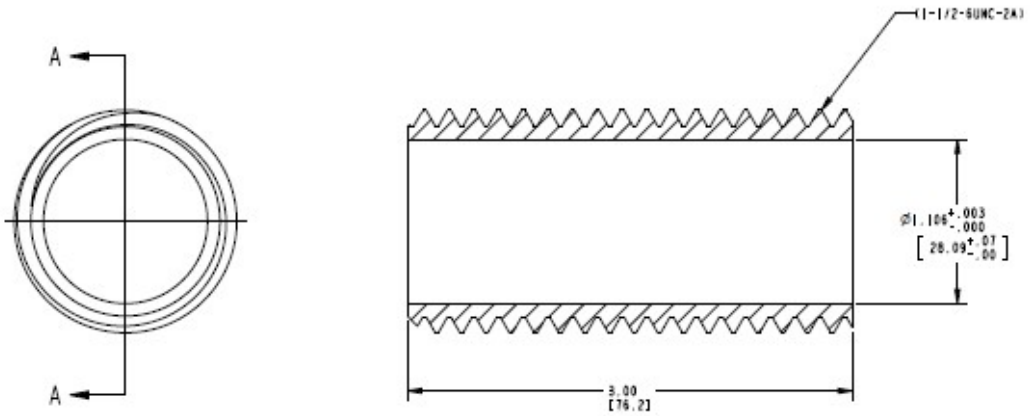

SECTION A-A
SCALE 2/1

-1 THREADED CONNECTION SLEEVE
5

Figure A-3. Support cradle and simply support fixtures

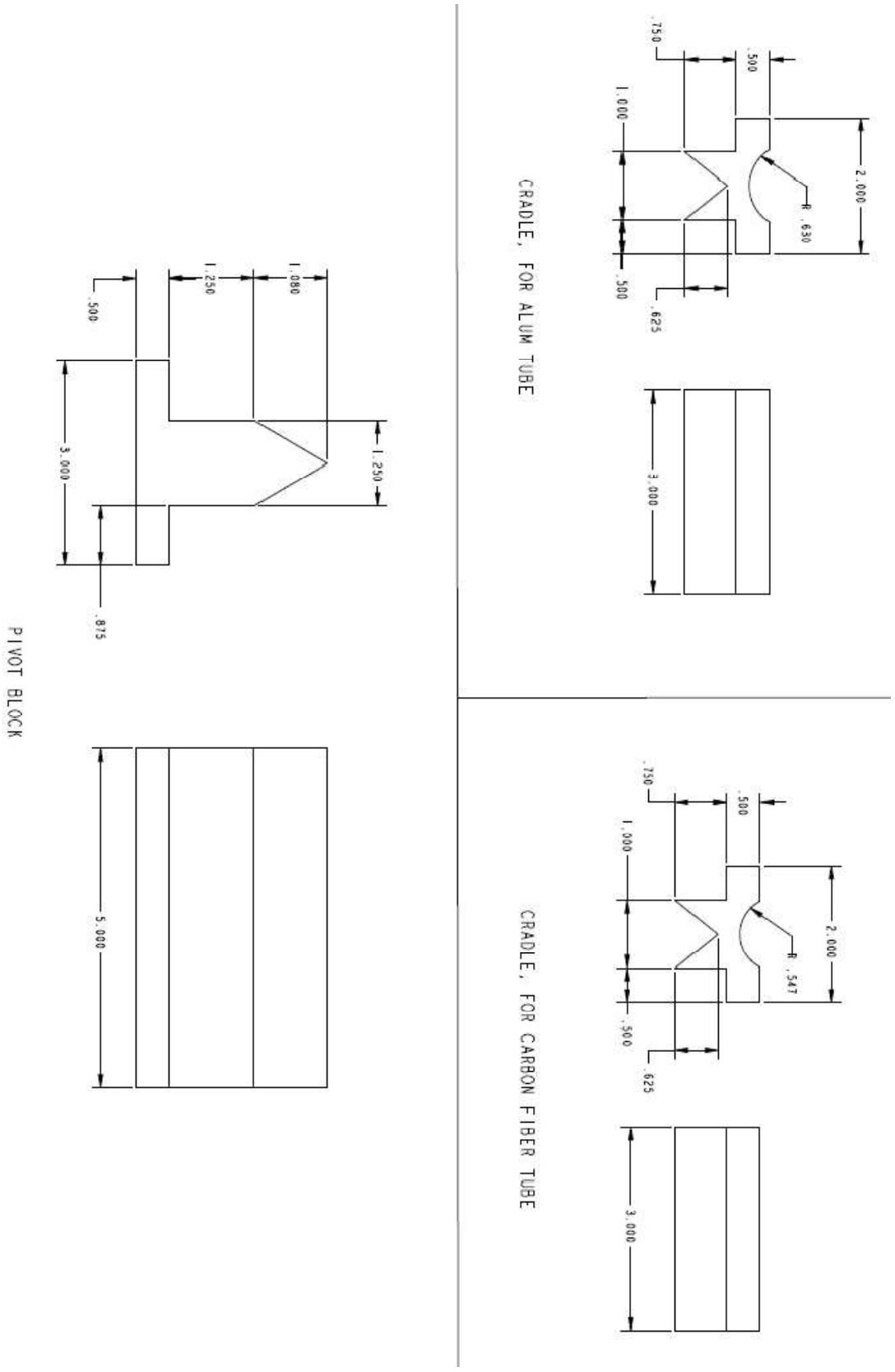

B. Bending Test Procedure

Test Procedure Up and Down

1. Assemble a multi-nut, a node without a composite tube, and two composite tubes with bonded node.
2. Add a screws and a load ring to the multi-nut for center LVDT measurements and loading.
    - Center deflection is measured from the top screw head.
3. Place the assembled test specimen on pivot cradles.
4. Check LVDT measurement points on the test specimen and reset the LVDT initial zero.
5. Add weigh on the test specimen with 5 lb increment, until the center deflection reaches 1 inch.
6. After the test, remove the screws and the load ring from the multi-nut.
7. Flip the test specimen and reattached the screw and the load ring to the multi-nut for the correct orientation.
8. Check the LVDT measurement points on the test specimen and reset the LVDT initial zero.
9. Add weigh on the test specimen with 5 lb increment, until the center deflection reaches 1 inch.
10. After the test, disassemble the screws, the load ring, the multi-nut, the node without a composite tube, and two composite tubes with bonded node.
11. Inspect and clean multi-nut fastener holes.

Test Procedure Side 1 and 2

1. Assemble a multi-nut, a node without a composite tube, and two composite tubes with bonded node.
2. Add two wing head screws to the multi-nut for center LVDT measurements and loading.
    - Center deflection is the average of two LVDT data from wing head screws.
3. Place the assembled test specimen on pivot cradles.
4. Check LVDT measurement points on the test specimen and reset the LVDT initial zero.
5. Add weigh on the test specimen with 5 lb increment, until the center deflection reaches 1 inch.
6. After the test, remove deformed shape of the test specimen by dissemble and reassemble multi-nut and composite tubes with node. Flip the test specimen.
7. Check the LVDT measurement points on the test specimen and reset the LVDT initial zero.
8. Add weigh on the test specimen with 5 lb increment, until the center deflection reaches 1 inch.

9. After the test, disassemble wing head screws, the multi-nut, the node without a composite tube, and two composite tubes with bonded node.
10. Inspect and clean multi-nut fastener holes.